Spring 1-1-2016

Experimental Study of Active Flow on a Photocatalytic Material for Air Quality Applications

Denise Catherine Mauney
University of Colorado at Boulder, denise.mauney@colorado.edu

Experimental Study of Active Flow on a Photocatalytic Material for Air Quality Applications

by

DENISE MAUNEY

B.E.D., Texas A&M University, 2013

A thesis submitted to the
Faculty of the Graduate School of the
University of Colorado in partial fulfillment
of the requirement for the degree of
Master of Science
Architectural Engineering
2016

This thesis entitled:
Experimental Study of Active Flow on a Photocatalytic Material for Air Quality Applications
written by Denise Catherine Mauney
has been approved for the Civil Environmental and Architectural Engineering Department

_____

Lupita D. Montoya

_____

Wil V. Srubar III

Date_____

The final copy of this thesis has been examined by the signatories, and we find that both the content and the form meet acceptable presentation standards of scholarly work in the above mentioned discipline.

Mauney, Denise Catherine (M.S., Architectural Engineering)

Experimental Study of Active Flow on a Photocatalytic Material for Air Quality Applications

Thesis directed by Assistant Professor Lupita D. Montoya

Experimental Investigation of Flow Field Patterns Resulting from Air Impingement by a Commercial Synthetic Jet Actuator on Wall Surfaces

The goal of this study was to characterize the flow field generated by a commercial, annular, multi-orifice synthetic jet actuator (SJA) as it impinged on a wall of varying surface textures. This experimental study determined the effect of SJA-to-wall distance on the airflow velocities near the impingement surface. The velocity profiles generated by the SJA were compared to those generated by a commercial axial computer fan (ACF) on smooth and rough surfaces. The results suggest that an SJA-to-wall distance of 215 mm had the greatest reduction on the peak airflow velocities, while an SJA-to-wall distance of 315 mm resulted in a velocity dampening effect furthest (225 mm) from the wall surface. Both the ACF and high-surface roughness resulted in increased turbulence at the wall surface. Increased surface roughness correlated to a decrease in the distance of the wall dampening effect.

Effect of Annular, Multi-Orifice Synthetic Jet Actuators on the Photocatalytic Degradation Rate of Nitrogen Dioxide (NO_2)

The effect of airflow velocities generated by an annular, multi-orifice synthetic jet actuator (SJA) and an axial computer fan (ACF) on the rate of photocatalytic degradation of nitrogen dioxide (NO_2) by a titanium dioxide (TiO_2)-doped reactive surface was experimentally studied in a closed chamber. The impact of flow characteristics generated by the SJA and ACF, namely surface velocity and velocity distribution across the reactor surface, on the removal rates was investigated herein. The results demonstrate that the use of active flow devices (SJA or ACF) enhanced the removal rate of NO_2 compared to ambient passive (control) conditions. However, increases in air velocity did not enhance the removal rate of NO_2. The highest removal rate (k=0.0013 min^{-1}) occurred when the SJA was located 315 mm from the reactor surface. This distance corresponded to a uniform surface velocity of approximately 0.1 m/s across the surface. A similar uniform surface velocity of approximately 0.1 m/s, when produced by the ACF, resulted in a lower removal rate (k=0.0011 min^{-1}) compared to the passive case. Thus, the unique flow characteristics of the SJA, in conjunction with its location at the optimized distance from the reactor, resulted in the greatest enhancement of the reduction of NO_2 by the TiO_2 reactive surface.

CONTENTS

LIST OF TABLES

LIST OF FIGURES

CHAPTER 1
OVERVIEW

This thesis is comprised of two experimental studies. It is divided into five chapters beginning with the thesis organization in Chapter 1, followed by the first and second experimental studies, which are presented in Chapters 2 and 3, respectively. Chapter 4 outlines recommendations for future work. References can be found in Chapter 5.

Chapter 2 presents an experimental study of the impingement of airflow generated by a synthetic jet actuator (SJA) and an axial computer fan (ACF) on a wall surface. The objective of the study was to characterize the air velocities near the surface of the wall as a function of (a) the distance between the active flow device and the impingement wall and (b) wall texture.

Chapter 3 presents an experimental study on the impact of airflows generated by SJA and ACF on the photocatalytic degradation rate of nitrogen dioxide (NO_2) *via* a titanium dioxide (TiO_2)-doped reactive surface. The objective was to determine the optimal distance to enhance the removal rate of NO_2. Results from this study were analyzed and informed by the results from Chapter 2 in order to determine the impact of surface velocity and flow characteristics on NO_2 removal rates.

This was the first evaluation of this commercial synthetic jet actuator for air quality control applications in buildings. Results herein suggest that the use of this low-power device has the potential to reduce energy-intensive ventilation requirements and improve overall occupant health and comfort.

CHAPTER 2
EXPERIMENTAL STUDY OF SYNTHETIC JET IMPINGEMENT ON A WALL SURFACE

2.1 Introduction

2.1.1 Air Quality in Buildings

High performance buildings require greater air tightness than conventional building codes demand and, consequently, special attention to indoor ventilation requirements. Reducing infiltration leads to higher demands for conditioning outside air for ventilation and can lead to an overall increase in heating and cooling loads (Chenari et al., 2016; Jokisalo et al., 2009; Ng et al., 2015; Emmerich and Persily, 1998), especially as climate change effects increase (Le et al., 2015). Some modern building materials have introduced a variety of pollutants, including volatile organic compounds (VOCs) as well as highly reactive molecules and radicals such as ozone, nitrogen oxides, hydroxyl radicals, and sulfur dioxides (Ulde and Salthammer, 2007), into the indoor environment. Reducing pollutant emissions from building materials increases both actual and perceived indoor air quality (Wilkins, et al., 2007; Wolkoff, et al., 1997). Sick Building Syndrome (SBS) is a term used to diagnose buildings where occupant exposure to indoor pollutants has led to negative health effects (Burge, 2004; Maddalena et al., 2015; Lu et al., 2016) and productivity losses. Studies have shown that improving indoor air quality in U.S. buildings can save $30 billion annually by reducing occupant sick days (Fisk, 2002). Traditionally, indoor air quality has been improved by increasing ventilation using energy-intensive central HVAC systems. Thus, methods and means to achieve acceptable building air quality without costly energy usage have become increasingly attractive.

Task/ambient conditioning (TAC) systems have been proposed as an alternative for improving indoor air quality in buildings, for example, individually controlled under-floor air distribution and desk-level supply air diffusers (Daly, 2002; Webster, Bauman, and Reese, 2002). Small scale, localized air cleaning systems serving as pollutant sinks can also alleviate energy demand on large-scale central systems particularly in geometrically complex interiors (Ning et al., 2013; Park et al., 2015).

2.1.2 Synthetic Jet Actuators (SJA)

Considered zero net mass flux devices, synthetic jet actuators (SJAs) are mechanical devices used to generate air flows that require zero mass input and produce non-zero momentum output (Glezer et al., 1998). An advantage of SJAs over conventional fans is that, since SJAs do not require mass input, they can be mounted to surfaces, requiring less space, while providing a greater heat transfer rate (Shaikh et al., 2016). These characteristics make SJAs desirable for electronic applications (Shaikh et al., 2016). Figure 1 shows a schematic of a SJA, where (a) the oscillating motion of a diaphragm (driven by piezoelectric, mechanical, or magnetic means) in the SJA cavity alternates between (b) suction and (c) ejection of fluid through the orifice. This process creates a continuous synthetic jet where the vortices are comprised entirely of ambient air. When a vortex is ejected through the orifice, it is propagated downstream and new ambient air is entrained into the cavity.

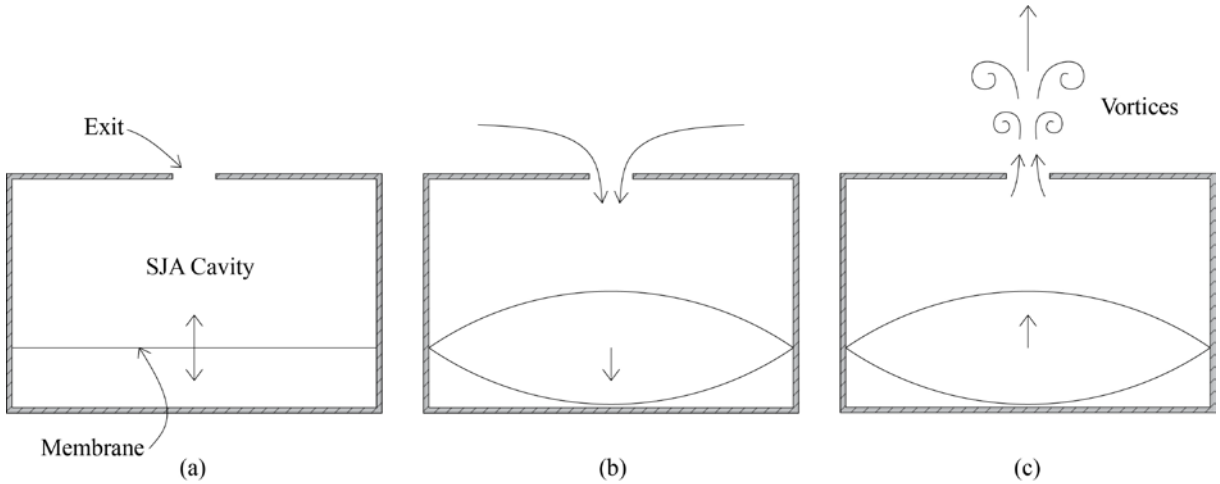

Figure 1 - Basic schematic of a SJA: (a) with deflecting membrane at rest, (b) pulling air in, and (c) ejecting air out and imparting a net momentum to the flow.

Synthetic jets have been used to enhance natural convection, especially for cooling purposes (Chaudhari, Puranik, and Agrawal, 2011; Arik and Setlur, 2009; Lasance and Aarts, 2008). According to Lasance and Aarts (2008), for similar heat transfer performance compared to conventional fans, synthetic jets provide lower noise levels, better thermodynamic efficiency (half the power or less), better form factor for design needs, higher reliability, less fouling, better scalability, and simple noise cancellation.

Synthetic jets have also been used to vector air streams and manipulate fluid flow (McQuillan et al., 2014; Tamburello and Amitay, 2008; Pavlova, Otani, and Amitay, 2008; Smith and Glezer, 1998) as well as

aerosols (Montoya et al., 2010; Allard 2011; Ziegler 2007) with no additional energy input. Synthetic jets entrain surrounding ambient air, altering the base flow on scales that are magnitudes larger than otherwise possible (Smith and Glezer, 1998). Also, by operating near resonance conditions, they achieve high efficiency with very little power input (Pavlova and Amitay, 2006).

Synthetic jets have been used extensively in heat transfer research listed above (Mahalingam and Glezer, 2005; Pavlova and Amitay, 2006; Chaudhari et al., 2011; Shaikh et al., 2016). Synthetic jets can generate highly agitated flow fields, enhancing the heat transfer rates with low power input. Pavlova and Amitay (2006), for example, found that, at the same Reynolds numbers, synthetic jets provided up to three times more cooling from surfaces than continuous jets due to the enhanced mixing generated by the coherent vortex rings formed by the synthetic jets. They found that synthetic jets operating at a frequency of 1200 Hz removed heat better than synthetic jets operating at a frequency of 420 Hz for small distances (up to H/d=12.5 to 16), where H is the distance between the synthetic jet orifice and the impingement wall and d is the diameter of the slot cavity opening. The 420 Hz jet was more efficient at larger distances up to H/d=28.

Chaudhari et al., (2011) experimentally investigated multi-orifice synthetic jets (with a center orifice surrounded by satellite orifices) and found that heat transfer coefficients using this device were 12 times those of natural convection and up to 30% more when compared to traditional single orifice synthetic jets. Their results also indicated that multi-orifice synthetic jets enhanced heat transfer, as the Nusselt (Nu) number grew in proportion with increased convection and turbulence.

Travnicek and Tesar, (2003) experimented with annular synthetic jets for impinging flow mass transfer. Annular synthetic jets operated at low frequencies retained their individual vortices for a larger distance compared to high frequency jets. They determined that the flow fields of low-frequency jets are dominated by a large recirculation bubble of a separated flow reaching up to the impingement wall.

Experimental studies have also compared synthetic jets to continuous jets. Smith and Swift (2003), for example, showed that for the same Reynolds number, synthetic jets were wider, slower, and had more momentum than similar continuous jets due to enhanced entrainment.

The results presented here (Chapter 2) form the basis for the experimental study presented in Chapter 3, where airflows generated by a SJA were used to enhance the removal of NO_2 by a TiO_2 photocatalytic surface. No known study has reported the impact of near-surface velocity on photocatalytic removal rate of NO_2 by TiO_2. However, near-surface velocity has been studied to measure its impact on adsorption/desorption rates of materials. While some have found near-surface velocity (measured at 10 mm from the surface) to have no impact on sorption rates (Jorgensen, Bjorseth, and Malvik, 1999), others have found that for some materials, sorption rates increase with an increase in velocity (Kjaer and Tirkkonen, 1996; Zhang, Zhang, and Chen, 2002). In general, the velocities tested in these studies ranged from 0.1 m/s to 0.3 m/s and were generated by a traditional fan. In Chapter 3, the further characterization of the SJA with respect to its ability to enhance the removal rate of TiO_2 will provide insight into whether SJAs provide a low-power alternative solution to traditional axial fans.

2.2 Materials and Experimental Methods

2.2.1 Synthetic jet actuator (SJA)

A low-frequency, annular, multi-orifice synthetic jet (SynJet ZFlow 87 LED Cooler) was purchased from Nuventix Inc. (Austin, TX). The flow range and field of this synthetic jet were characterized in previous work (Abarr et al., 2016). The device is comprised of 8 annular slots, each 2 mm wide and evenly spaced around the perimeter of the SJA face, as shown in Figure 2a. The power consumption of the device is 0.46 W, with a current draw of 38 mA at 12 V. A 12 V DC power supply provides a sine wave current load that is two times the actuator displacement to account for both positive and negative directions of the diaphragm. The frequency is estimated between 100-120 Hz. The range is caused by the reduction of 12 V DC to 5 V for internal SynJet use. While synthetic jets can be noisy and, according to Arik and Setlur (2009), can reach 65 dB, the SynJet model used in this study has a maximum noise level of 27 dBA and a silent performance mode of 19 dBA.

2.2.2 Axial computer fan (ACF)

The flow fields of a 12VDC, 40 mm axial computer fan (ACF), model number 70-4128 of LKG Industries, Rockford, IL, were also partially analyzed in this study. Figure 2b shows a computer aided design representation of this device. The ACF power consumption is 0.96 W, with a current draw of 0.80 mA at 12 V. The fan has 7 blades of 10 mm wide and a blade pitch of 44.3 degrees.

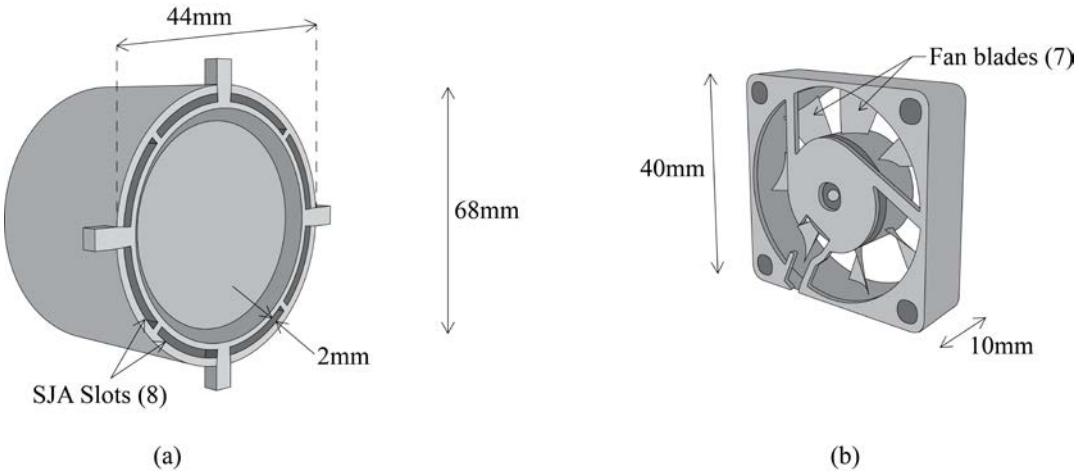

Figure 2 – Dimensioned CAD Representation of: (a) Nuventix SynJet ZFlow 87 LED Cooler, and (b) LKG Industries Axial Computer Fan.

2.2.3 Anemometer

A hot wire anemometer (Climomaster Model 6531, Kanomax, Andover, NJ) with an accuracy of 0.1 m/s was used to measure air velocity. The anemometer recorded 40, one-second measurements at each location and reported the average velocity and standard deviation.

2.2.4 Impingement wall surfaces

Three wall surface textures were studied to determine their effect on the peak velocity (at the center line) generated by the synthetic jet: 1) a smooth, polished stainless steel sheet (900x900 mm), 2) a medium-grade (150 grit, 228 x 279 mm) 3M-brand sandpaper sheet, and 3) a coarse sandpaper sheet (100 grit, 228 x 279 mm). The sheets were attached flush to the wall using an adhesive and placed perpendicular to the impinging flow of air. The sheet metal served as the smooth “control” wall surface.

2.2.5 Experimental Setup

The modular system used to mount the SJA, ACF, and anemometer is described in Abarr et al. (2016) and is shown in Figure 3. The assembly can be adjusted in the x, y, and z directions. The hot wire

anemometer (probe) was positioned normal to the direction of airflow and it was moved in the x direction while the devices (SJA or ACF) remained at a fixed L distance from the wall (Figure 4). Flow fields were determined by moving the SJA or ACF in the y and z directions at each L distance.

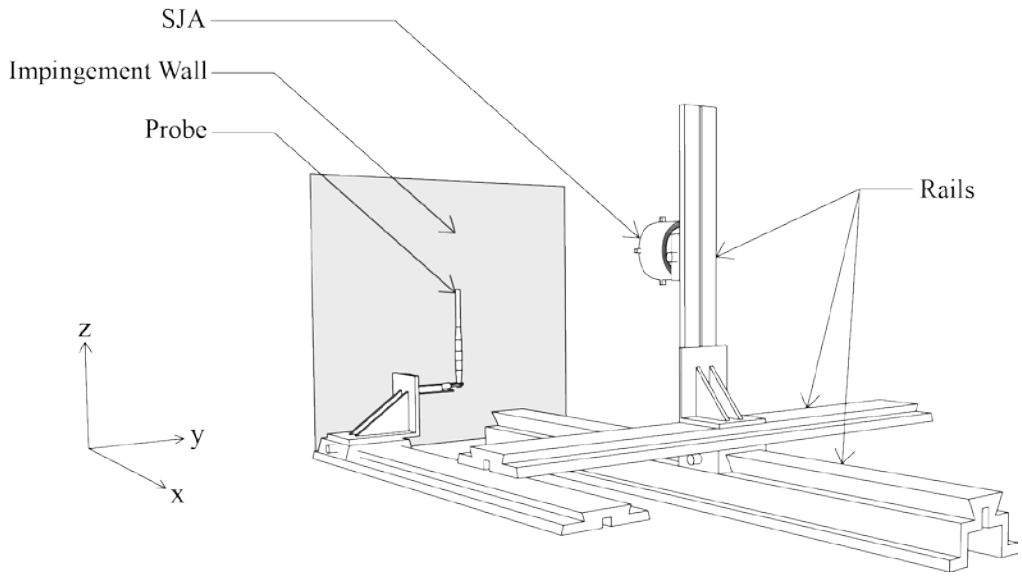

Figure 3 – Experimental Setup for Impinging Flow Study

Prior to each experiment, the center of the surface, the anemometer hot wire, and the SJA were aligned. For each experiment, the device (SJA or ACF) was placed at a fixed distance from the wall (L= 115, 215, 315, 510, 760, 1010 mm). Next, the probe was placed at a distance x from the wall (x = 10, 20, 30, 50 mm) as shown in Figure 4. Once both the L and x locations were finalized, then the velocity profile for that location was determined. First, the SJA or ACF was moved in the +/- y direction to complete the "y-velocity profile" and then moved in the +/- z direction to complete the "z-velocity profile."

Therefore, for each L-distance, multiple y and z velocity profiles were measured at varying x-distances from the impingement surface (x=10, 20, 30, 50 mm) (Figure 4).

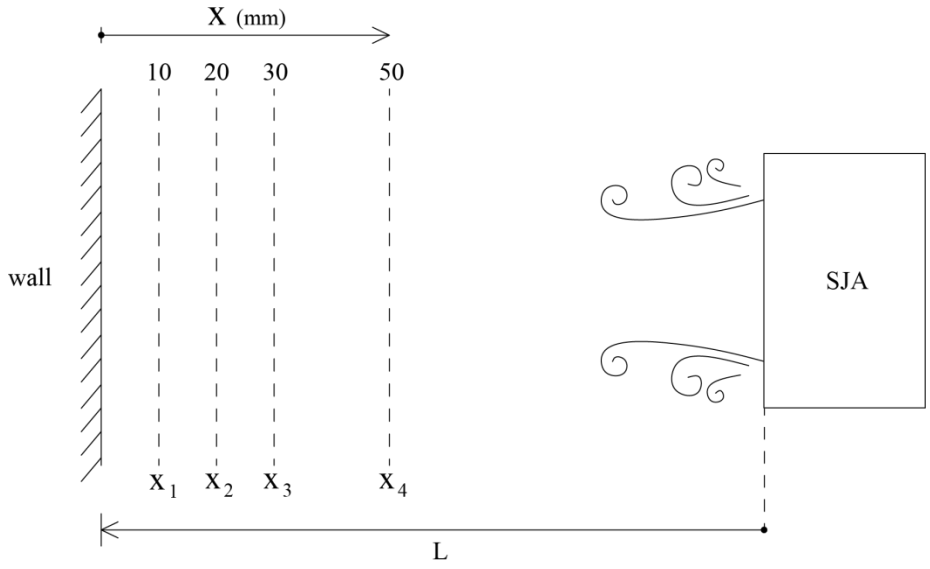

Figure 4 - Schematic of L and x Testing Positions

For instance, at a distance of L=115 mm, y and z velocity profiles were determined at x=10 mm (the distance from the wall) and was denoted as x_1 (Figure 4). The subsequent y and z profiles of x_2, x_3 and x_4 followed at x=20, 30, and 50 mm, respectively. The SJA and anemometer were moved in 10 mm increments for all directions. Table 1 shows the complete list of L and x locations included in this study.

Table 1 – L and x Locations for Impinging Flow Experiments

	Distance from Wall surface to probe, x (mm)	L=115 mm	L=215 mm	L=315 mm	L=510 mm
		Distance from SJA orifice to probe (mm)			
x1	10	105	205	305	500
x2	20	95	195	295	490
x3	30	85	185	285	480
x4	50	55	155	255	450

The four planes of velocity data (at x_1, x_2, x_3 and x_4) for each L distance determined the overall shape of the flow field near the impingement surface. In this study, x-profiles refer to data points taken along the x-axis at the centerline of the SJA and were also referred to as “peak” velocities.

2.2.6 Experimental Objectives

2.2.6.1 Effect of SJA-to-wall distance on peak velocity

In the first investigation, the impact of the wall presence on the peak (center, y=0, z=0) velocity was determined at six different distances (L) between the synthetic jet and the wall surface. The objective was to characterize how the air velocities at each location were affected by the presence of a surface located perpendicular to the airflow (Figures 3 and 4). This characterization was necessary and in preparation for future studies on pollutant removal enhanced by localized ventilation. In those studies (Chapter 3), airflows generated by the SJA were directed towards removal surfaces (i.e., wall).

2.2.6.2 Characterization of velocity profiles near impingement wall

The second investigation determined the velocity profiles near the impingement wall (x= 10, 20, 30, 50 mm from the wall) when the device (ACF or SJA) were located at L= 115, 215, 315, 510, 760, 1010 mm from the wall. The purpose was to characterize how the shape of the velocity profiles parallel to the wall surface changed with the SJA-to-wall distance (L). These findings were to inform future experiments about how gaseous air pollutants behave when directed towards a removal surfaces by localized directed airflows.

2.2.6.3 Flow field patterns of ACF vs. SJA

The third investigation was identical to the investigation described in section 2.2.6.2, except that the SJA was replaced with an axial computer fan (ACF). The objective was to characterize the shape of the velocity profiles parallel to the wall surface and compare them to the SJA velocity profiles at the corresponding distances from the wall (L).

2.2.6.4 Impact of surface roughness on velocity profiles near impingement wall

Given that materials for airborne-pollutant removal include porous, non-porous, coarse and fine textures, the fourth investigation characterized the impact of surface roughness on velocity profiles near the wall surface.

2.3 Results and Discussion

2.3.1 Impact of wall presence on peak velocity

In order to determine the impact of the wall surface on the SJA flow, airflow velocities were measured along the centerline axis with and without an impingement wall. Figure 5a depicts the centerline axis velocity measurements (x-profile) without the presence of a wall. The following Figures 5b-5g show the x-profiles with and without the wall at each fixed L distance (115, 215, 315, 510, 760, 1010 mm).

In Figure 5a, the velocity exhibited a maximum of 1 m/s at approximately 60 mm from the SJA orifice. The measurements from within the first 60 mm from the orifice, which exhibited the lowest magnitudes, are representative of non-converged airflow. At 60 mm from the orifice, the vortices of the eight individual annular slots converge (vortex convergence point). Travnicek and Tesar (2003) found that annular synthetic jets with an electrical input of 0.16 W and low excitation frequency of 120 Hz experienced vortex convergence at a distance of approximately 1.5D to 2D, where D is the diameter of the synthetic jet from one slot across the orifice to another (Travnicek and Tesar, 2003). By this definition, the expected convergence point for the annular SJA used in this study was approximately 96-128 mm from the orifice face. The actual convergence point was found to be 60 mm, as shown in Figure 5a. It should be noted that the SJA used in this study has a greater number of annular slots than the comparison study, and this geometric dissimilarity may have led to the difference in the expected vs. actual convergence points.

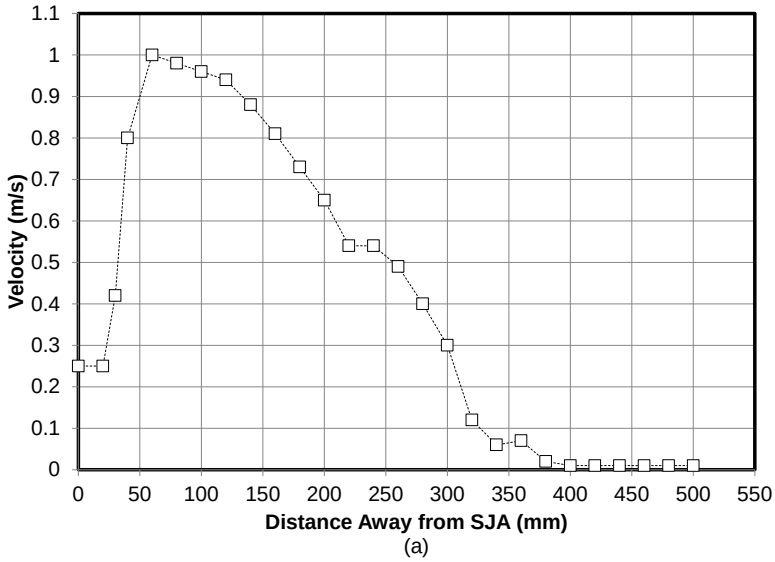
Velocity (m/s)
Distance Away from SJA (mm)
(a)

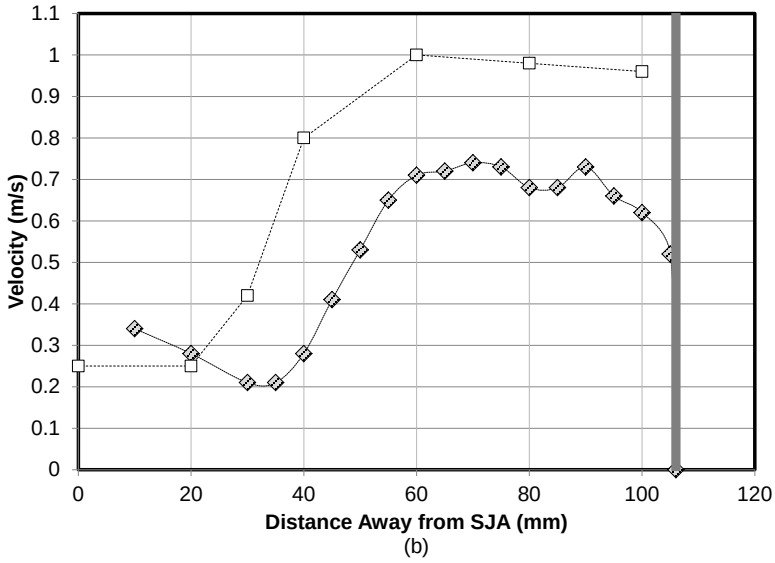
Velocity (m/s)
Distance Away from SJA (mm)
(b)

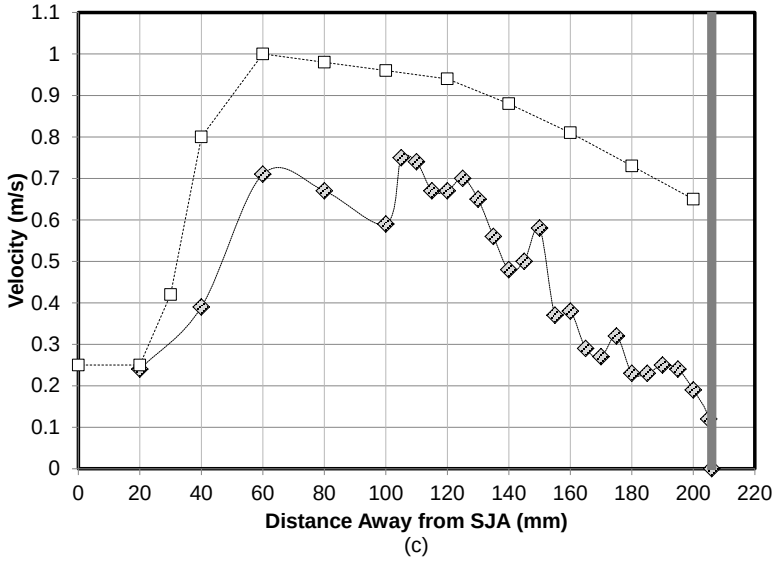
Velocity (m/s)
Distance Away from SJA (mm)
(c)

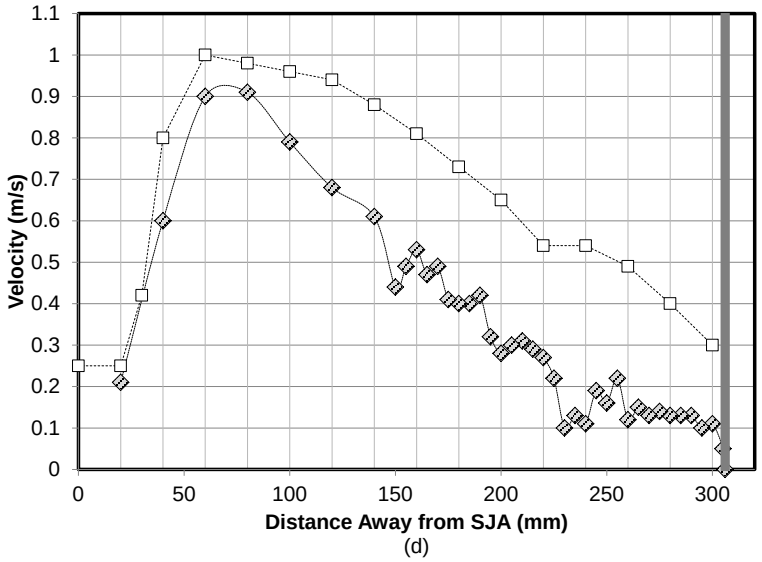
Velocity (m/s)
1.1
1
0.9
0.8
0.7
0.6
0.5
0.4
0.3
0.2
0.1
0
0
50
100
150
200
250
300
Distance Away from SJA (mm)
(d)

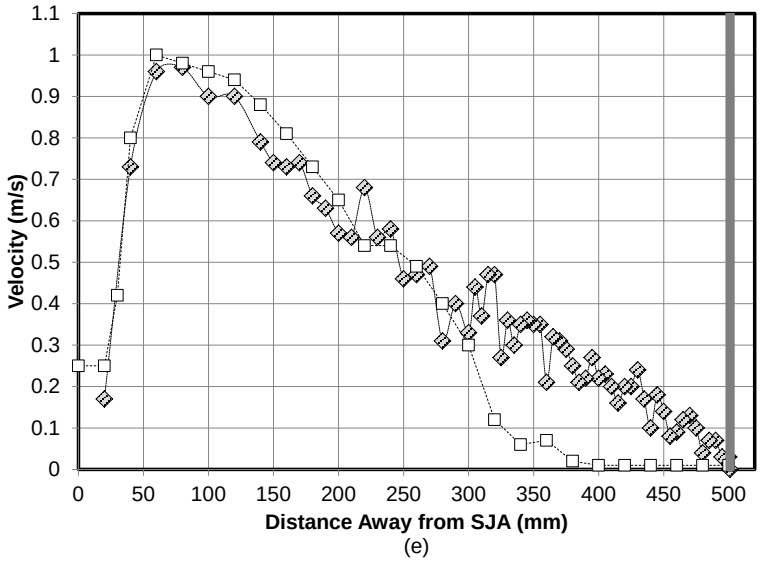
Velocity (m/s)
1.1
1
0.9
0.8
0.7
0.6
0.5
0.4
0.3
0.2
0.1
0
0
50
100
150
200
250
300
350
400
450
500
Distance Away from SJA (mm)
(e)

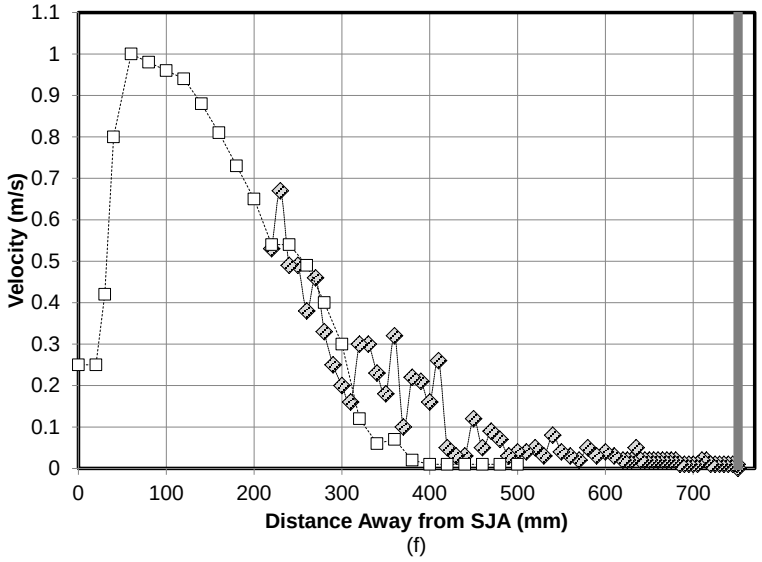
Velocity (m/s)
1.1
1
0.9
0.8
0.7
0.6
0.5
0.4
0.3
0.2
0.1
0
0
100
200
300
400
500
600
700
Distance Away from SJA (mm)
(f)

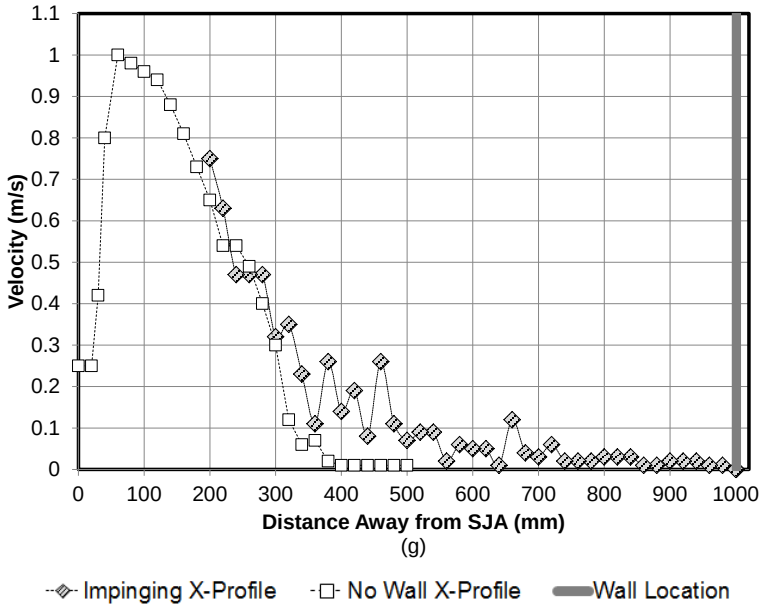

Figure 5 – SJA X-Profile Velocities: (a) No Wall, (b) L=115 mm, (c) L=215 mm, (d) L=315 mm, (e) L=510 mm, (f) L=760 mm, and (g) L=1010 mm

Figure 5b shows the x-profile of the SJA at L=115 mm along with the x-profile of the SJA without the impingement wall. The wall had a dampening effect on the magnitude of the velocities at L=115 mm. The presence of the wall reduced the velocity by an average of 0.33 m/s. Figure 5c shows the x-profiles for the SJA at L=215 mm with and without the wall present. The wall had a dampening effect on the magnitude of the velocities for a range of approximately 185 mm from the wall surface. The presence of the wall reduced the velocity by an average of 0.38 m/s. Figure 5d shows the x-profile of the SJA at L=315 mm with and without the wall present. The wall had a dampening effect on the magnitude of the velocities for a range of approximately 225 mm from the wall surface. The presence of the wall reduced the velocity by an average of 0.29 m/s. Figure 5e shows the x-profile of the SJA at L=510 mm with and without the wall present. The wall had a dampening effect on the magnitude of the velocities for a range of approximately 200 mm from the wall surface. The presence of the wall reduced the velocity by an average of 0.16 m/s. Figure 5f shows the x-profile of the SJA at L=760 mm with and without the wall present. The wall had no measurable dampening effect on the magnitude of the velocities. Figure 5g shows the x-profile of the SJA

at L=1010 mm with and without the wall present. The wall had no measurable dampening effect on the magnitude of the velocities.

Table 2 summarizes the impact of the presence of the wall on all SJA x-profile velocity measurements. The "range of wall impact" refers to the distance, in mm, from the wall at which the velocity measurements of the two data sets (with and without the wall) show negligible differences (<0.1 m/s). These results were used to determine at what SJA location the wall could be considered to have negligible impact. Avg. reduction in velocity is defined as the average reduction in velocity on the SJA x-profiles with the wall present as compared to the SJA x-profile without the wall present. At L=510 mm, the velocities nearest the wall were greater than the velocities without the wall present; thus, the wall had a positive impact on these velocities and it is denoted as a negative reduction (or increase) in Table 2.

Table 2 – Summary of Wall Impact on SJA X-Profile Velocity Measurements

L (mm)	Range of wall impact (mm)	Avg. reduction in velocity (m/s)	% reduction in velocity
115	105	0.33	54.4
215	185	0.38	55.6
315	225	0.29	55.7
510	200	-0.16	-393.9
760	0	*negligible**	0.0
1010	0	*negligible**	0.0

**negligible is defined as a difference of less than 0.1 m/s between the two data sets at all test points.*

The results indicate that at an SJA-to-wall distance of L=215 mm, the wall contributed to the largest reduction in velocity (0.38 m/s). At an SJA-to-wall distance of L=315 mm, the wall reduced the airflow velocities up until a distance of 225 mm away from the wall. This was the greatest range of wall impact. In the SJA-to-wall position of L=315 mm, the wall produced a similar % reduction in airflow velocity to L=115 mm and L=215 mm. An SJA-to-wall distance greater than or equal to L=760 mm exhibited less than 0.1 m/s delta between the wall and no-wall data sets. Here the wall is considered to have no measureable impact. At L=315 mm, the wall not only had the largest measurable range of impact at 225

mm, but it also had a dampening effect on the airflow velocities nearest the wall (Figure 5d). For a range of 80 mm from the impingement surface, the air velocity is steadied at approximately 0.13 m/s. This leveling effect is an interesting attribute of L distance and likely influences the quality of mixing experienced by the air nearest the surface.

2.3.2 Characterization of velocity profiles near impingement wall

In the previous section, the greatest range of wall impact was determined by examining the x-profile velocity data with and without an impingement wall. In this section, the range of wall impact in the radial (y and z) directions is further analyzed. It was predicted that a greater L distance between the SJA and the wall would lead to an increased breakup of the individual vortices and, thus, more uniform velocity values across the surface of the wall. Travnicek and Tesar (2003) found that low-power, low-frequency annular impinging synthetic jets, such as the one used in this study, retained stable individual vortices up to a distance equal to that of the slot diameter (D). For larger distances, the annular SJA's vortices undergo a breakup before reaching the wall, and upon impact, become turbulent. All L distances included in this study exceeded the slot diameter D (64 mm); therefore, it was expected that in all cases, the individual vortices broke up before reaching the wall surface.

Figures 6-9 show the velocity profiles created by the SJA near the impingement surface (x_1, x_2, x_3, x_4). The data series x_1 through x_4 represent four separate velocity profiles parallel to the wall surface. The x_1 velocity profile is closest to the wall surface while x_4 is furthest from the wall surface. Refer to Figure 4 for the locations of each of the x_1 through x_4 velocity profiles from the wall.

At L=115 mm, velocities exceeded 0.4 m/s at the centerline axis on x_1. There was a well-defined peak velocity around the center, indicating greater definition and separation of individual vortices impacting the wall. At approximately 50 mm from the centerline axis, the velocities in all profiles decreased sharply. The profile closest to the SJA (x_4) exhibited two peaks that were created by individual vortices leaving opposing annular jet slots. These vortices remained distinct at this distance (x_4, 50 mm) from the wall.

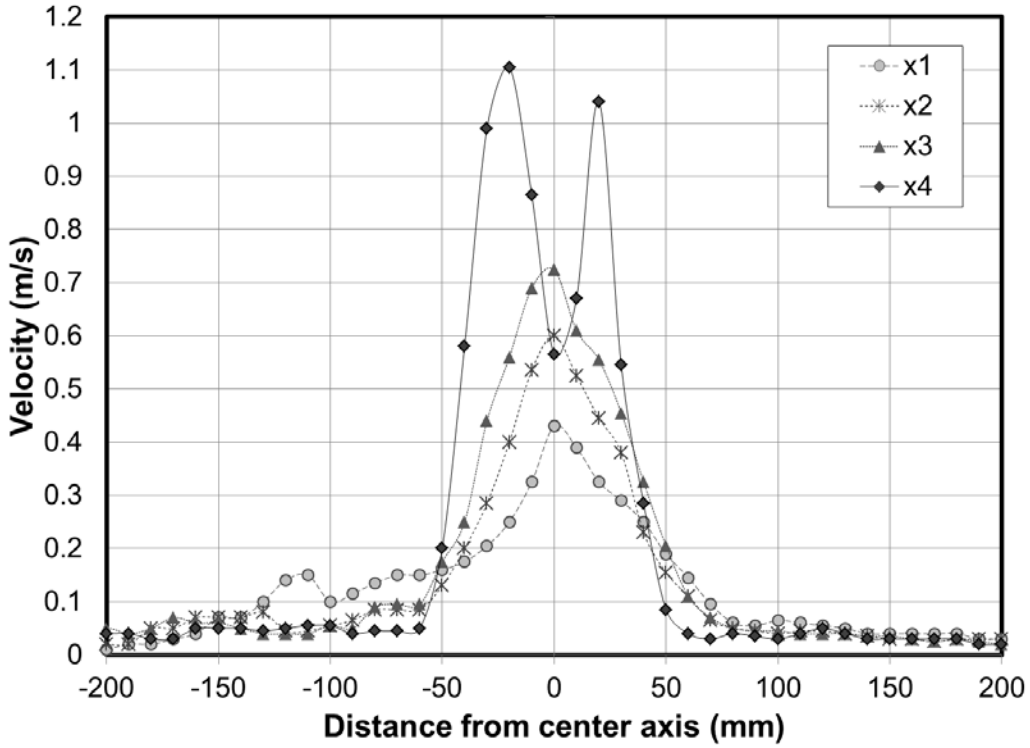

Figure 6 – SJA Near-Surface Velocity Profiles at L=115 mm

Expectedly, at L=215 mm (Figure 7), the velocity profiles x_1-x_4 were more similar in magnitude compared to the x_1-x_4 velocity profiles of L=115 mm (Figure 6). These results indicate that individual vortices converge and experience a more significant breakdown near the surface. Along the centerline, the velocities averaged between 0.15 and 0.25 m/s.

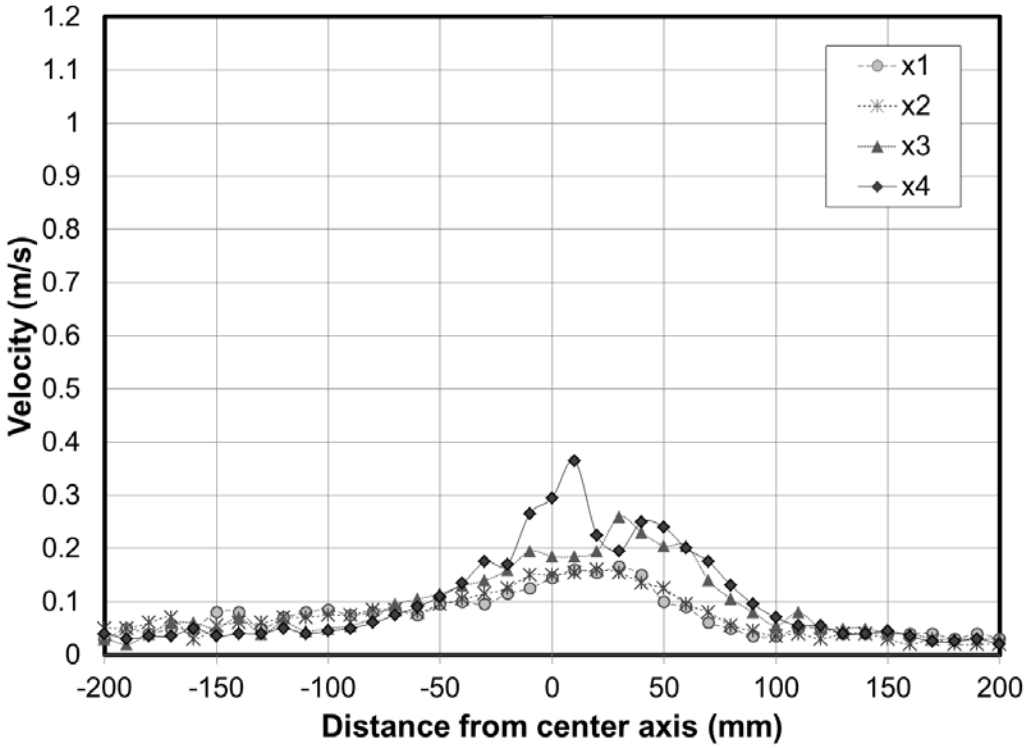

Figure 7 - SJA Near-Surface Velocity Profiles at L=215 mm

At L=315 mm (Figure 8), the velocity were more uniform farther away (100 mm) from the centerline. While the profiles at L=315 mm resulted in a similar shape to those of L=215 mm (Figure 7), there was no clear velocity peak at the centerline. At this L distance, it is evident that the vortices converge further from the wall and, thus, spread further in the radial directions.

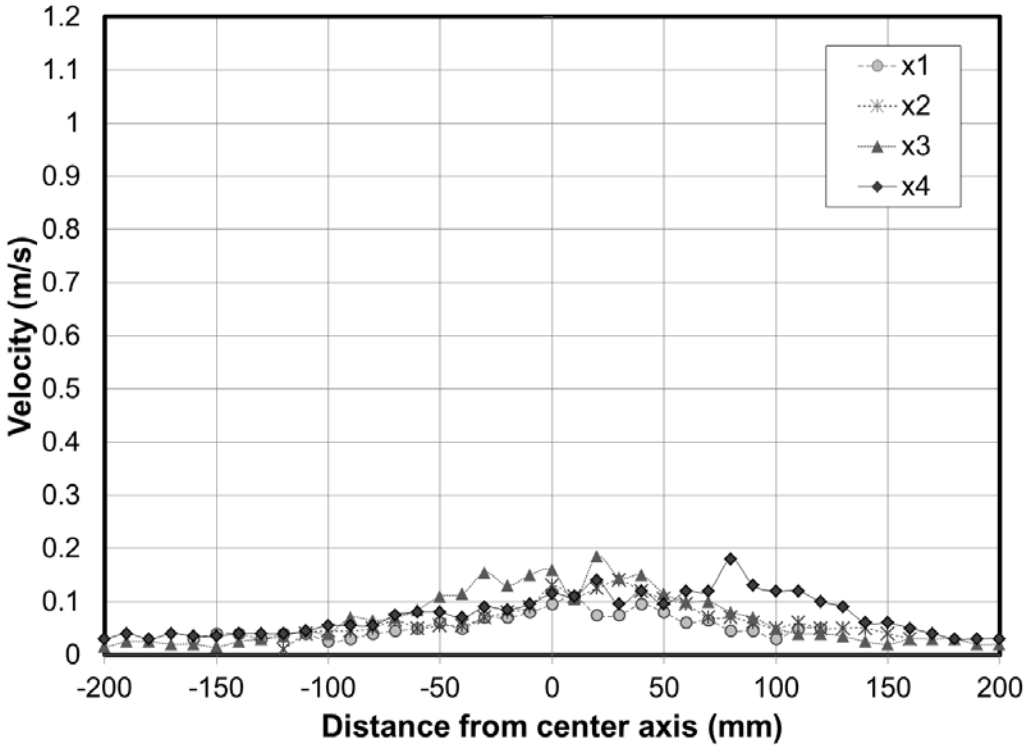

Figure 8 - SJA Near-Surface Velocity Profiles at L=315 mm

At L=510 mm (Figure 9), while all velocity measurements were within the margin of error of the anemometer (<0.1 m/s), similar patterns to Figures 6-8 were exhibited. The velocity profiles spread further in the radial directions due to vortex convergence far from the wall surface.

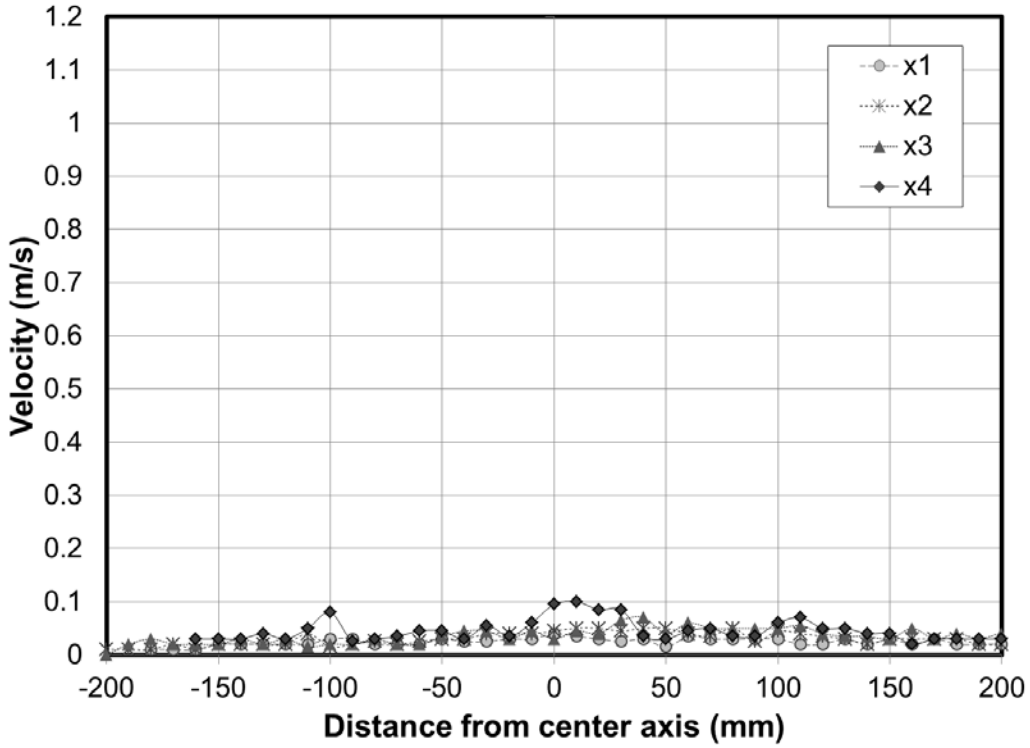

Figure 9 - SJA Near-Surface Velocity Profiles at L=510 mm

At distances L=315 mm and L=510 mm, the results indicate significant breakdown in vortices prior to impingement. This created a flow field near the impingement surface that was more uniformly distributed in the radial directions as compared to the distinct velocity profiles of x1 through x4 at L=115 mm. At L=315 mm the peak velocity at the centerline was no longer distinguishable, and, at L=510 mm, the velocity was almost uniform across the surface.

According to Chaudhari et al. (2011), the average Nusselt number (for heat transfer) increases with an increase in Reynolds number. As discussed in their study of multi-orifice synthetic jets, Chaudhari et al. (2011) discovered there are optimum (L/D) normalized axial distances (D is the slot orifice diameter) where the Nusselt number, and thus heat transfer, is maximized. A direct comparison is not possible among different synthetic jet geometries; however, there appears to exist an L distance where the slot diameter D produces an optimal profile for enhanced heat transfer. For our research, a potential optimal distance for air pollutant removal is of interest. Higher velocities indicate higher Reynolds numbers and

increased turbulence which enhances heat transfer. For pollutant removal, however, the effect of velocity is unknown; the goal of this research is to perform an initial evaluation. We hypothesized that a low (<0.2 m/s), uniform velocity across the impingement surface would define the optimal L distance for pollutant removal.

2.3.3 Flow field patterns of ACF vs. SJA

2.3.3.1 Results of ACF vs. SJA Flow Comparison

Figure 10 shows the x1-x4 velocity profiles for the ACF at a fixed distance of L=315 mm. The velocity profile x_1 (closest to the surface) showed a lateral spread of more than 150 mm in the radial (y) directions and exhibited uniform velocity of 0.1 m/s for a range of over 100 mm. In contrast, the SJA did not produce uniform velocity profiles. In Figure 5d L=315 mm, at x_1, the velocities are approximately 0.1 m/s only for a range of 50 mm. The velocity profiles of the SJA at x_2, x_3, and x_4 are nearly identical to x_1, indicating the wall influence is greater in the x-direction in the case of the SJA than in the case of the ACF. This is likely due to the unidirectional nature of the synthetic jet vortices, where the velocity measurements are more uniform and concentrated around the centerline axis. The flow generated by the ACF seems more turbulent and widespread. It is less affected by the presence of the wall at x_2, x_3, and x_4. Though it may seem that the center of the surface is experiencing the same conditions at x_1 for both devices, given the similar velocities, the remaining profiles (x_2, x_3, x_4) suggest overall dissimilar flow fields. For further details on the evaluation of these devices, see Abarr et al., (2016).

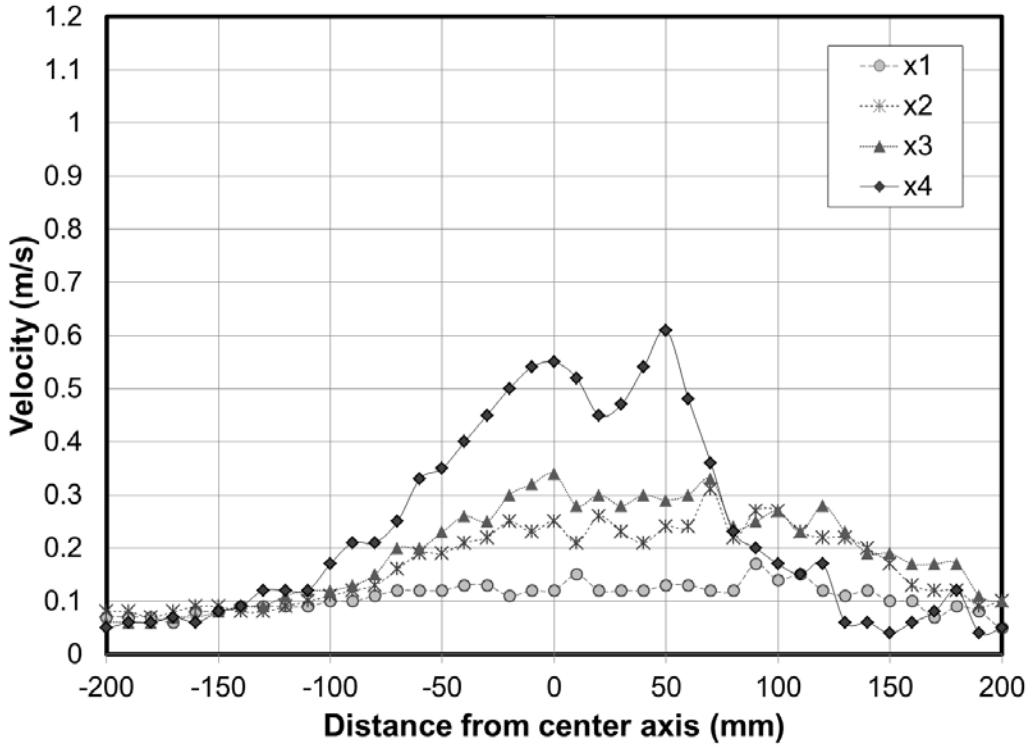

Figure 10 - ACF Near-Surface Velocity Profiles at L=315 mm

2.3.4 Impact of surface roughness on velocity profiles near impingement wall

The velocity profiles generated by the SJA near an impingement wall of different roughness were also determined. Sandpaper of medium and coarse roughness were used as textured replacements for the solid sheet metal (smooth) surface. Refer to Section 2.3.2 for the results of the smooth surface experiment. Figures 11 and 12 show the results of the coarse and medium sandpaper surfaces at an SJA-to-wall distance of L=315 mm. Refer to Figure 5d for the results of the smooth surface experiment at the SJA-to-wall distance of L=315 mm. The velocity profiles obtained when using a coarse surface are shown in Figure 11. The results are similar to the corresponding smooth surface SJA velocity profiles (Figure 5) with the exception of the data measured at the x_4 location. The coarse paper did not impact the magnitudes of the x_4 profile as much as the smooth surface. This is likely attributed to the grit of the sandpaper disrupting the perpendicular directional flow of the impinging vortices. The grit lessens the x-distance of the wall's impact on the airflow by distributing the flow energy in a randomized manner rather than directly reflecting the flow energy back in the direction of the device. It is similar to how the ACF

lessens the x-distance of the wall's impact because of the turbulent, non-directional nature of its flow. As shown in Figure 12, no noticeable differences were evident between the medium grit and coarse grit sandpaper, suggesting that the change in grit size between medium and coarse sandpaper was not large enough to impact airflow velocities by magnitudes greater than 0.1 m/s.

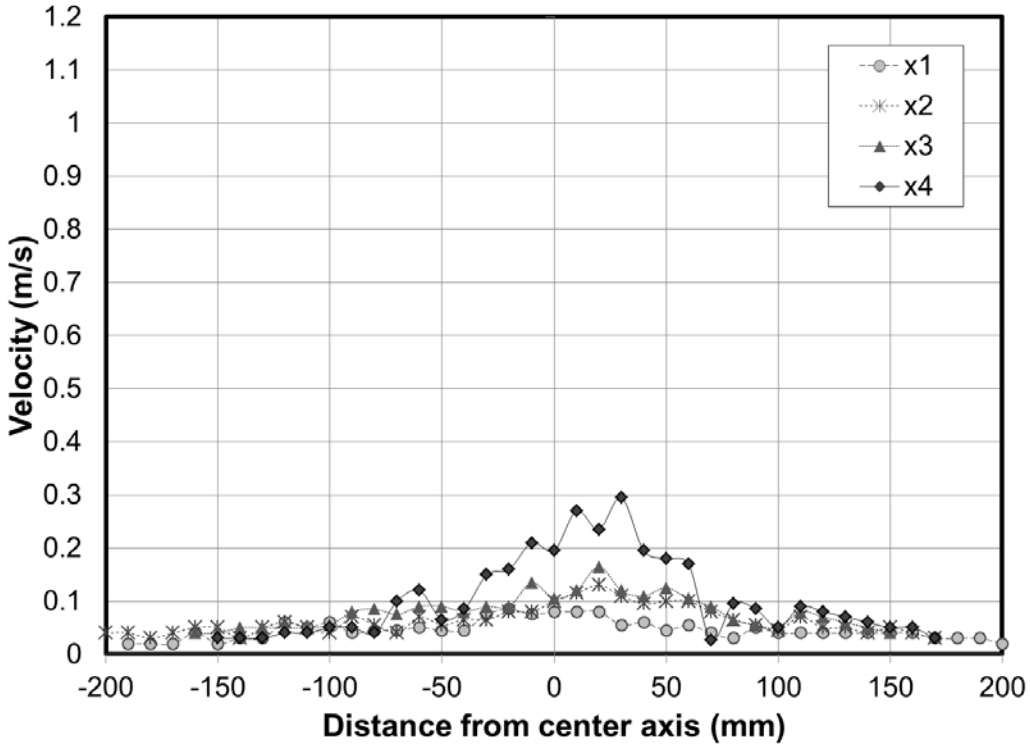

Figure 11 – Velocity profiles generated near a coarse surface at L=315 mm

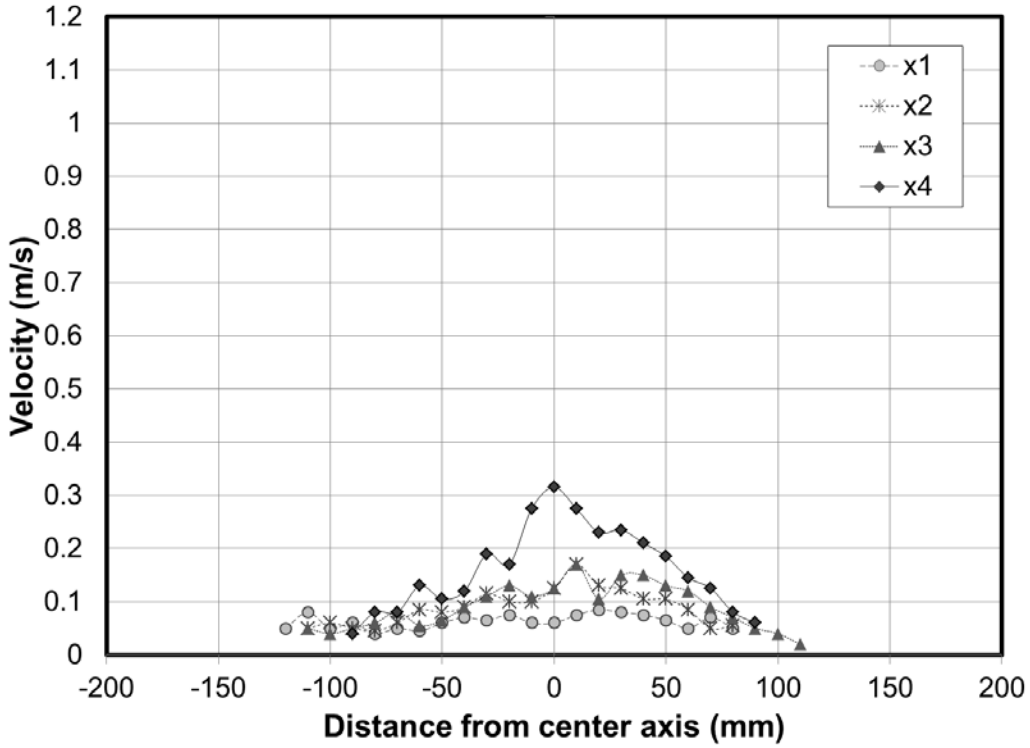

Figure 12 – Velocity profiles generated near a medium coarse surface at L=315 mm

2.4 Conclusions

The objective of the study was to characterize the air velocities near the surface of the wall as a function of (a) the distance between the active flow device and the impingement wall and (b) wall texture. Results for the SJA suggest that the impingement surface has the greatest impact on the magnitude of the x-profile airflow velocities at a distance L=215 mm, which corresponded to an average velocity reduction of 55.6%. At L=315 mm, the wall exhibited the greatest distance, or range, of impact by reducing airflow velocities up to 225 mm in the x-direction from the wall surface. In addition, it was found that the impingement surface has no measureable impact at distances L > 760 mm. Comparative analysis between the airflow velocity profiles of SJAs and ACFs and the impact of surface roughness on SJA airflow showed that increased turbulence at the impingement surface was generated by highly agitated ACF flow and by the presence of a rough texture on the impingement surface. The kinetic energy of the SJA flow perpendicular to the surface was dissipated radially amidst the rough surface instead of back towards the active flow device. In comparison to the ACF, the SJA exhibited greater unidirectional, concentrated flow

around the centerline axis because of the nature of its axisymmetric vortices. This can be leveraged for achieving targeted flow toward a specific point with the added advantage of greater dynamic pressure per unit input power. The results presented herein formed the basis for the experimental study presented in Chapter 3, where airflows generated by a SJA were used to enhance the removal of NO_2 by a TiO_2 photocatalytic surface.

CHAPTER 3
EFFECT OF AIRFLOWS GENERATED BY AN ANNULAR, MULTI-ORIFICE SYNTHETIC JET ACTUATOR ON THE PHOTOCATALYTIC DEGRADATION RATE OF NO_2

3.1 Introduction

The experimental study presented in Chapter 2 is a characterization of the velocity flow fields created by a synthetic jet actuator (SJA) and a small axial computer fan (ACF) impinging on a wall at varying distances from the wall surface. Chapter 3 presents an experimental investigation on the impact of airflows generated by that SJA on nitrogen dioxide (NO_2) removal rate by a photocatalytic titanium dioxide (TiO_2)-doped surface reactor. The active flow devices, a SJA and ACF used in Chapter 2, were used in the experiments presented here. The results of the characterization of the velocity flow fields in Chapter 2 were then used to analyze, correlate, and explain the results obtained here in Chapter 3. Specifically, they showed how the velocity flow fields created by the active flow devices affected the removal rate of NO_2 by the TiO_2 photocatalytic surface.

3.1.1 Effect of air velocity on pollutant sorption processes

Several previous studies have determined the impact of air velocity on volatile organic compounds (VOC) sorption in building materials (Zhang et al., 2002; Kjaer and Tirkkonen, 1996; Jorgensen et al., 1999). As expected, the differences in building materials and pollution compounds used in these studies have led to a wide array of results. For example, Jorgensen et al. (1999) reported negligible effects of velocity on ∝-pinene and toluene sorption on wool carpet. Zhang et al. (2001) found that increased air velocity had insignificant effect on the sorption of most test compound and material combinations except for dodecane on carpet, where increased air velocity led to increased sorption. Due to the lack of statistical significance of the effect of air velocity on sorption for the majority of those experiments, Zhang et al. (2002) concluded that it is not possible to form a general consensus on the impact of velocity on VOC sorption. Knudsen, Kjaer, Nielsen, and Wolkoff (1999) studied three floor coverings, an acrylic sealant, and wall paint on gypsum board to determine the impacts of air velocity on VOC emissions (desorption) from

commonly used building materials. They found that after an initial period of up to 14 days, the emission rate of VOCs was independent of air velocity. They found, however, that if the building product surface is sensitive to oxidative degradation, increased air velocity may result in increased secondary emissions (originally chemically or physically bound VOCs). Similarly, Kjaer and Tirkkonen (1996) found that, for gypsum board, the desorption rate of a mixture of 17 compounds increased as velocity increased.

3.1.2 Nitrogen Dioxide

Nitrous oxides (NO_x) are a family of highly reactive gases formed when fuel is burned at high temperatures. A nitrogen oxide of concern is nitrogen dioxide (NO_2), a brownish gas and powerful oxidizing agent that reacts in air to form nitric acid, toxic organic nitrates, and ozone. The greatest sources of NO_x in ambient air come from vehicles, fossil fuel power generation, and industrial boilers. NO_2 is also formed naturally by lightning, plants, soil, and water (USEPA, 2010); however, only about 1% of the total NO_2 in ambient city air is formed in this way. Ambient NO_x levels are regulated in part, to minimize atmospheric reactions that generate ozone, a potential respiratory hazard. In 2010, the National Ambient Air Quality Standard (NAAQS) was revised to include a new standard for a 1-hour average maximum level of NO_2 outdoors. This regulation served to supplement the existing annual standard, which alone failed to consider the danger of short-term bursts of exposure to the harmful gas. Although no standard exists for indoors, incidents of harmful exposure have been known to occur near gas stoves and other household gas appliances. The current NAAQS standard for outdoor nitrogen dioxide is a 53 ppb (0.053 ppm) annual mean and a 100 ppb 1-hour average.

NO_2 is a lung irritant that can lower resistance to respiratory infections (USEPA, 2010). Increased levels of NO_2 can impact asthma sufferers by inducing more frequent and intense attacks, especially in children (Cibella et al., 2015) and hospitalizations (Carugno et al., 2016). A study by Tunnicliffe, Burge, and Ayres (1994) found that concentrations of NO_2 in homes can slightly heighten the response of asthmatic patients to allergens. Recently, it has been shown that exposure to NO_2 can induce chronic and acute changes in lung function (Cibela et al., 2015; Latza et al., 2009), including bronchial neutrophilic

infiltration (Barck et al., 2005; Delfino et al., 2006, Kampa and Castanas, 2008). Although ambient (outdoor) levels of NO_2 in the U.S. have decreased 60% since 1980, its adverse health effects have received increased attention, especially those produced by indoor sources of NO_2 that contribute to the 1-hour ambient limit (USEPA, 2010). Short spikes of NO_2 in indoor environments can be attributed to unvented fuel-burning appliances (e.g., gas cookers), heating appliances (e.g., poorly maintained boilers and kerosene heaters), and tobacco smoke (Franklin et al., 2006). A study in Portage, Wisconsin found that, although ambient outdoor levels of NO_2 ranged between 7 and 27$\mu g/m^3$, NO_2 levels in kitchens with gas stoves were approximately 50$\mu g/m^3$ higher than outdoor concentrations (Spengler et al., 1983). In contrast, kitchens in electric-cooking homes had NO_2 levels below the outdoor concentrations (Spengler et al., 1983). Improperly vented gas appliances were most often found in homes of people with lower socio-economic status, especially those located in cold-weather heating climates. In general, indoor NO_2 levels in gas-cooking homes were higher in winter and lower in summer due to seasonal changes in air exchange rates (Lai et al, 2006; Franklin et al., 2006; Spengler et al., 1983). It has also been shown that in children, indoor NO_2 increases the risk of asthma (Cibela et al., 2015) and increases the risk of current wheeze (Lin, Brunekreef, and Gehring, 2013). Belanger et al. (2013) found that asthmatic children exposed to NO_2 indoors, at levels well below the US Environmental Protection Agency outdoor standard (53 ppb), are at risk for increased asthma morbidity.

3.1.3 Photocatalysis of NO_2 using Titanium Dioxide (TiO_2)

It has been shown that NO_2 can be photocatalytically converted to other stable compounds when exposed to titanium dioxide (TiO_2) (Beeldens, Cassar, and Murata, 2011; Boonen and Beeldens, 2014). The photocatalytic process has made TiO_2 desirable for its air cleaning abilities (Maury et al., 2007; Aghighi and Haghighat, 2015). Since TiO_2 is chemically stable, relatively inexpensive, self-regenerative, and the photogenerated holes are highly oxidizing, TiO_2 makes a good candidate for environmental air quality research (Fujishima and Zhang, 2006).

The photocatalytic process for TiO_2 consists of three main phases: exposure, oxidation, and removal (Hashimoto et al., 2005). When exposed to UV light (hv), TiO_2 is activated and electrons are released near the surface. These electrons bind with oxygen to form super oxide anions, leaving the surface of TiO_2 positively charged. This surface then takes electrons from the moisture in the air; the water molecules then become hydroxyl radicals. Both the hydroxyl radicals and the super oxide anions can oxidize pollutants in the air. A precipitate is then left on the surface of the material. These precipitates may be removed from the material with water (e.g., rain) (Hashimoto et al., 2005).

It has been shown that the reaction of nitrogen monoxide (NO) in the presence of TiO_2 produces nitric acid (HNO_3) (Boonen and Beeldens, 2014; Katsanaki et al., 2013). NO is photocatalytically converted via nitrous acid (HNO_2) to yield NO_2. NO_2 is then oxidized by a hydroxyl radial to produce HNO_3. NO_2, discussed further in this section, is, therefore, an intermediate product of NO reactions with TiO_2 (Boonen and Beeldens, 2014). Incomplete catalysis of NO may lead to increased concentrations of NO_2 (Boonen and Beeldens, 2014). One study found that when TiO_2 was exposed to formaldehyde, incomplete oxidation led to the net generation of formaldehyde (Hodgson, Destaillats, Sullivan, and Fisk 2007). NO_2 can also directly oxidize oxygen or organic materials.

Previous work with NO_2 photocatalytic degradation by TiO_2 has found that efficiency of NO_x reduction (%) increases with pollutant contact time (larger surface, lower velocity, higher turbulence) (Beeldens, Cassar, and Murata, 2011). In a study by Boonen and Beeldens (2014), the application of TiO_2 in concrete for air purification was found to be feasible and beneficial in urban environments especially due to its self-cleaning capabilities. Maggos, Bartzis, Leva, and Kotzias (2007) found that a decrease in relative humidity (from 50% to 20%) enhanced the photo-oxidation rate of NO on surface samples from 0.11 $\mu g/m^2 s$ to 0.42 $\mu g/m^2 s$. Toma, Bertrand, Klein, and Coddet (2004) found that when using TiO_2 as a photocatalytic oxidator, the NO_x removal increased proportionally with the area of the irradiated geometric surface. In general, larger surfaces, lower air velocities (< 2 m/s), lower relative humidity, and higher incident light angle have all enhanced pollutant reduction (Beeldens, Cassar, and Murata, 2011; Maggos, Bartzis, Leva, and Kotzias, 2007; Toma, Bertrand, Klein, and Coddet, 2004).

3.1.4 Titanium dioxide in building applications

When properly applied, self-cleaning materials can save time and maintenance, which are important factors in the lifetime of building components. One study in Japan found that TiO_2 tiles that cladded a building must only be cleaned every 5 years, which is much less frequent than traditional filtration air-cleaning devices (Fujishima and Zhang, 2006). This frequency depends on many factors, including illumination, amount of rainfall, and accumulation rate of soiling, which can affect the material's ability to self-regenerate. Perhaps the greatest advantage of photocatalytic materials in general is that they can be added easily to construction materials, making them practical to implement into infrastructure projects.

3.1.5 Byproducts

The gaseous byproducts generated from the reaction of NO_2 with a TiO_2 surface under UV irradiation include nitrous acid (HONO), nitrogen monoxide (NO), and nitrous oxide (N_2O). These gases are harmful respiratory irritants. All of these compounds are known to cause health effects at certain levels. In a study by Bedjanian and Zein (2012), HONO was produced as a byproduct in the presence of O_2 at temperature range of 280K-320K.

HONO undergoing photocatalysis produces OH radicals, which are responsible for the formation of ozone and secondary organic compounds such as VOC oxidation products. Catalytic properties of TiO_2 surfaces are directly involved in – and impacted by – HONO production (Langridge et al., 2009). Consequently, as photolysis of HONO occurs, it significantly reduces TiO_2 surface efficiency for NO_x removal by 40-70% (Langridge et al., 2009). If building materials contain TiO_2, there is potential concern for the effectiveness of NO_x ($NO + NO_2$) removal because of the described byproducts.

3.1.6 Scope of Work

The experimental study presented here investigates the photocatalytic degradation of NO_2 by a TiO_2-doped reactive surface in a closed chamber. In addition, forced local ventilation, provided by a commercial synthetic jet (SynJet ZFlow 87 LED Cooler) is applied to promote this degradation. There are

no known experimental studies conducted with the commercial SJA used in this work for air quality applications. Further, this is the first experimental study investigating the removal of NO_2 gas using a photocatalytic reacting surface and localized ventilation (created by the SJA) in a closed chamber. Specifically, there are no previous studies that investigate the effect of air velocity on NO_2 removal by a TiO_2-doped surface.

When compared to the ACF (LKG Industries m#70-4128), one advantage of the SynJet ZFlow 87 LED Cooler SJA is that it is able to produce greater dynamic pressure per unit input power (Abarr et al. 2016). It is hypothesized here that the SJA can enhance pollutant removal rates over the ACF with less power input due to its unique flow field described in Chapter 2. To test this hypothesis, a controlled, air-tight test chamber was built and used to conduct experiments to measure the impact of localized ventilation on the removal rate of NO_2 by the photocatalytic reactor surface. The active flow device was placed at predetermined distances (L=115, 215, 315, 510, 760, 1010 mm) from the TiO_2 reactor surface, which corresponded to those used in Chapter 2. The objective of this study was to determine the locations where each active flow devices produced the highest NO_2 removal rate. The SJA and the ACF were then compared in terms of removal rate enhancement. The results presented here integrate the surface velocities determined in Chapter 2.

3.2 Materials and Methods

3.2.1 Materials

3.2.1.1 Titanium dioxide-doped reactor surface

A round reactor surface with an area of 325 cm^2 (0.0325 m^2) made of cement mortar and doped with TO_2 on the surface was custom-made in our laboratory for this study. The reactor was prepared using 687 g sand, 250 g cement, and 121 mL water. The cement mortar reactor was then dusted with TiO_2 powder to create a TiO_2-doped surface and allowed to cure for 7 days before removed from the mold.

3.2.1.2 Ultraviolet lamp

The UV lamp used in this experiment was a 26 W no-heat compact fluorescent lamp (ZooMed ReptiSun m# FSC10) with a 30% UVA, 10% UVB, full spectrum output. The lamp was housed in a deep-dome lamp fixture with a highly polished aluminum inside surface to maximize concentrated output. In the study by Toma et al., (2004), a 15 W bulb with ultraviolet fraction of 30% UVA and 4% UVB was used for photocatalytic removal of nitrous oxides. Others have used 25 W fluorescent tubes, which emit 100% UVA radiation in the range of 300-400 nm (Ballari, Hunger, Husken, and Brouwers, 2010).

3.2.1.3 Low intensity illumination

For this study, the UVA/UVB radiation was fixed at a surface average of approximately 3 $\mu W/cm^2$. An average illuminance of 3 $\mu W/cm^2$ on the reactor surface is representative of indoor environments exposed to typical fluorescent lighting or ambient daylighting (Fujishima, Rao, and Tyrk, 2000). In indoor environments, this irradiation level can be achieved if the TiO_2-doped material is placed approximately 10 feet from a window with an overcast sky (Fujishima, Rao, and Tyrk, 2000). By using natural sources of UVA/UVB radiation, this experimental setup could be implemented in a building. The photocatalytic effect of TiO_2 depends on the energy of the incident photons, not on their intensity (Fujishima et al., 2000); therefore, a small number of photons with the required amount of energy can incite photocatalytic reactions with TiO_2. Low intensity illumination from typical indoor fluorescent lighting can also supply the required UV light energy needed to induce photocatalysis; however, in the presence of low-intensity illumination, the photocatalytic material removed only about 10 ppmv of pollutant (Fujishima et al., 2000).

3.2.1.4 Experimental chamber setup

The chamber used for this experiment (Figure 13) was constructed with 3/16" (4.76 mm) clear acrylic and enclosed a volume of 0.69 m^3 (0.80x0.80x1.08 m). The top of the chamber was hinged on one side to allow access into the chamber. The TiO_2 reactor area was designed to be <5% of the chamber cross-sectional area, which minimized the effect the wall had on the airflow velocities measured over the

reactor surface. The dimensions were selected to comply with the required wind tunnel blockage ratio specified by ASTM D5116 (ASTM International, 2013). Inlet and outlet ports were sealed with silicone gel, and the hinged lid was sealed with soft silicone rubber and clamps. The UV light was placed approximately 30" away from the TiO_2 reactor just outside the chamber, as shown in Figure 13.

A toxic gas probe (Graywolf m#TG-502) was used to measure NO_2 concentration, relative humidity (RH), total volatile organic compounds (TVOC), O_3, and NO inside the chamber. The sensor can detect NO_2 at a range of 0 to 20 ppm with a resolution of 0.01 ppm (http://www.wolfsense.com/pdf/specs/electrochemicals.pdf). The NO_2 monitor was placed 200 mm from the right wall of the chamber and in line with the SJA and reactor, as shown in Figure 13.

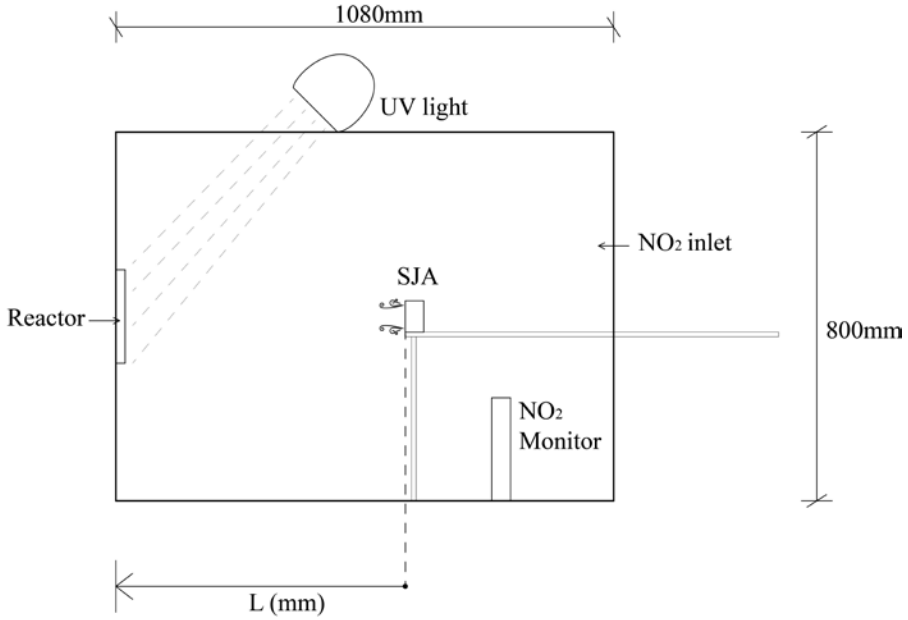

Figure 13 – Experimental Chamber Setup and Dimensions

3.2.2 Experimental Methods

Prior to experimentation, the air-tightness of the chamber was evaluated using two methods: monitoring the chamber pressurization and measuring CO_2 concentration in the chamber over time. The first method involved measuring the airflow rate needed to reach a steady pressure difference across the chamber walls at prescribed flow rate increments. The second method involved measuring the concentration of CO_2 as a tracer gas inside the chamber over time. CO_2 was injected into the chamber and measured using a portable

emissions monitoring system (PEMS, Aprovecho Research Center, Cottage Grove, OR) over a period of one hour.

To conduct the actual experiments on the photocatalytic degradation of NO_2, the following protocol was followed. The NO_2 monitor, TO_2 reactor, and active flow device (SJA or ACF) were securely positioned inside the chamber, as shown in Figure 13. Measurements from the monitor were allowed to stabilize for 15 minutes prior to closing and sealing the chamber. Once the chamber was sealed, the active flow device was turned on to mix the air inside the chamber. After reaching a steady NO_2 concentration reading of approximately 0.3 ppm, a small puff of NO_2 was pumped into the chamber from a Teflon bag. Once a steady concentration of approximately 0.48 ppm was achieved, the UV light was turned on to activate the TO_2 reactor. In the control experiment, the active flow device was turned off before the UV light was turned on. In all other trials, the active flow device was left on for the remainder of the experiment. These conditions were held constant for three hours in the closed chamber system. After three hours, the UV light was turned off and the chamber was flushed with clean air for approximately one hour. For all trials, the temperature and RH inside the chamber were remained at 73°F and 17%, respectively, with a maximum deviation of 1.5°F and 2.8%, respectively. The experiment was independently repeated three times at each testing location and in a randomized order.

The removal of NO_2 in this study was assumed to be a first-order reaction as follows:

$$\frac{-\mathrm{d}[\mathrm{NO_2}]}{\mathrm{dt}} = \mathrm{k}[\mathrm{NO_2}] \tag{2}$$

The integrated first-order rate law is

$$\ln[\mathrm{NO_2}] = -\mathrm{kt} + \ln[\mathrm{NO_2}]_0 \tag{3}$$

The removal rate, *k*, of the reactor, defined in units of min^{-1}, was determined as the slope of the straight line when $\ln[NO_2]$ is plotted vs. time, t.

3.3 Results and Discussion

3.3.1 Chamber air-tightness

The result of the air-tightness test by pressurization is shown in Figure 14. A linear correlation between pressure difference and flow rate in two repeated trials was obtained, indicating that the chamber was able to maintain a constant pressure with less than 1% variation in the flow rate at each step. The error bars represent the standard deviation. Figure 15 shows the results of the air-tightness of the chamber using the CO_2 concentration method over time. The test maintained a level of 950 ppm CO_2 after its injection for the duration of the test (one hour). Therefore, the results from both methods indicated that chamber leakage was negligible, or below 0.001 L/min.

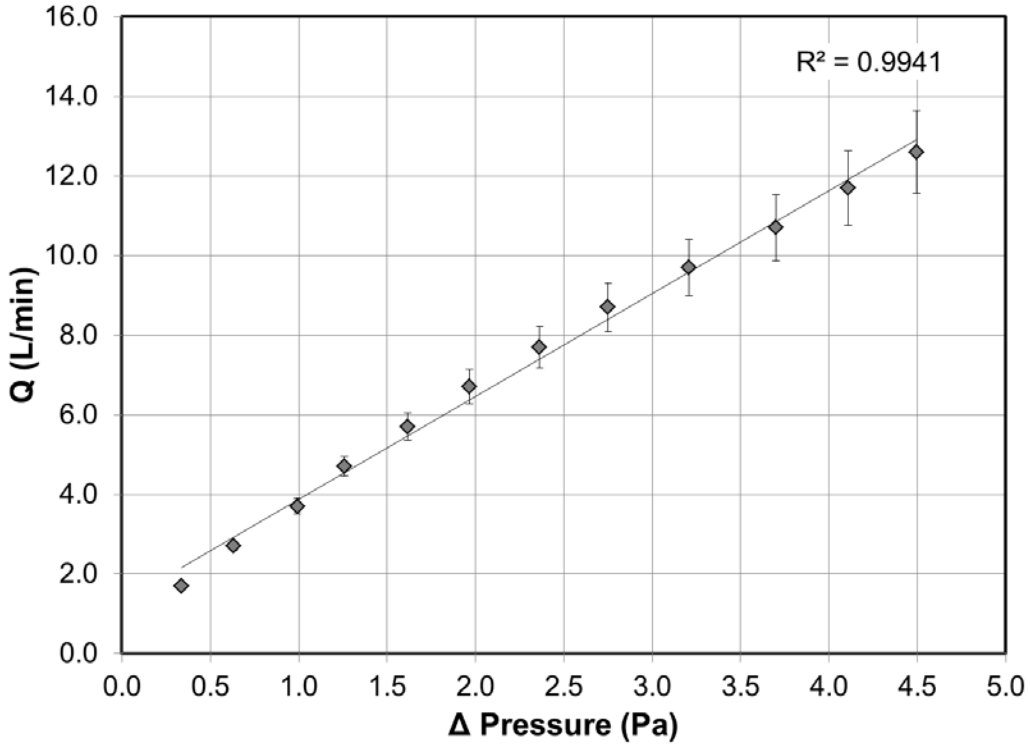

Figure 14 – Determination of Chamber Air-tightness by Pressurization

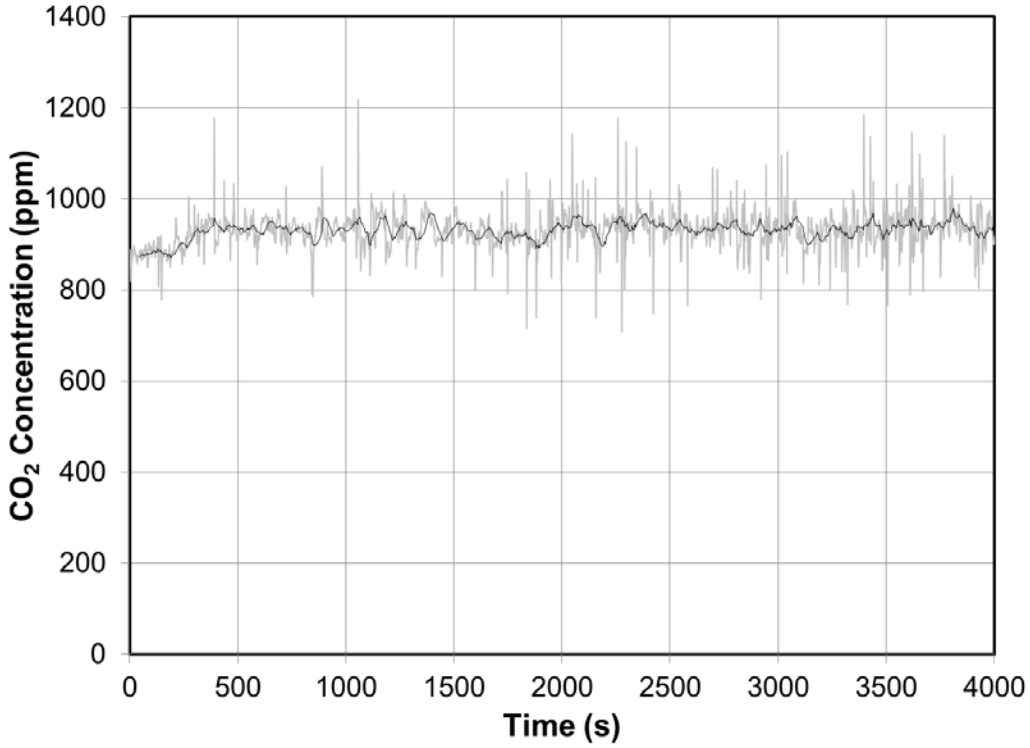

Figure 15 – Determination of Chamber Air-tightness by CO_2 Concentration over Time

3.3.3 Impact of distance from surface on pollutant removal

Figure 16 shows the control test where no active flow device was used. The solid squares represent the average $\ln(C_{NO2}(t))$ over time for three separate trials while the error bars represent the maximum and minimum values from the three trials. The NO_2 removal rate is represented as (-k), or the slope of the trend line, in units of 1/min (m^{-1}). Larger *absolute k* values represent greater, or better, removal rates of NO_2. The control experiment (Figure 16) resulted in a removal rate of k=-0.0007 min^{-1}, which corresponds to a 12.5% reduction in NO_2 concentration over a period of three hours.

Figures 17 through 19 show the results of the NO_2 removal by the TiO_2-doped surface at three separate SJA-to-wall distances (L=115, 315, 510 mm). The greatest removal rate achieved was k=-0.0013 min^{-1} at an SJA-to-wall distance of 315 mm, which corresponds to a 19.27% reduction in NO_2 concentration from the chamber over a period of three hours (Table 4). It also corresponds to a photocatalytic removal rate, as described by Maggos et al. (2007), of 0.034 $\mu g m^{-2} s^{-1}$.

Maggos et al. (2007) studied the photocatalytic removal rate of NO_2 by commercial paints containing TiO_2. Their pollutant removal rate was measured as photocatalytic oxidation rate (PR), in $\mu gm^{-2}s^{-1}$. Maggos et al. (2007) were able to reach a PR of 0.11 $\mu gm^{-2}s^{-1}$ in the case of water-based styrene acrylic paint treated with 10% TiO_2, exposed to one hour of UV irradiation and exposed to an initial concentration of 220 ppb NO_2. The initial concentration in the current study was approximately twice as high (480 ppb); also, the mass of TiO_2 used in the current study was likely greater (but unknown). Both initial concentration of NO_2 and mass of TiO_2 have been shown to increase photocatalytic removal (Knudsen et al., 1999; Toma et al., 2004; Fujishima et al., 2000). However, the greatest PR produced by this study at L=315 mm was 0.034 $\mu gm^{-2}s^{-1}$, which is likely much less than the PR found by Maggos due to the difference in UV light intensity. The current study used an average illuminance of 3 $\mu W/cm^2$ (0.3 W/m^2) on the reactor surface while Maggos et al. (2007) used 4.6 W/m^2 in the center of the reactor and 2.1 W/m^2 near the edges. This difference represents about 14 times more UV light in the experiments by Maggos et al. (2007).

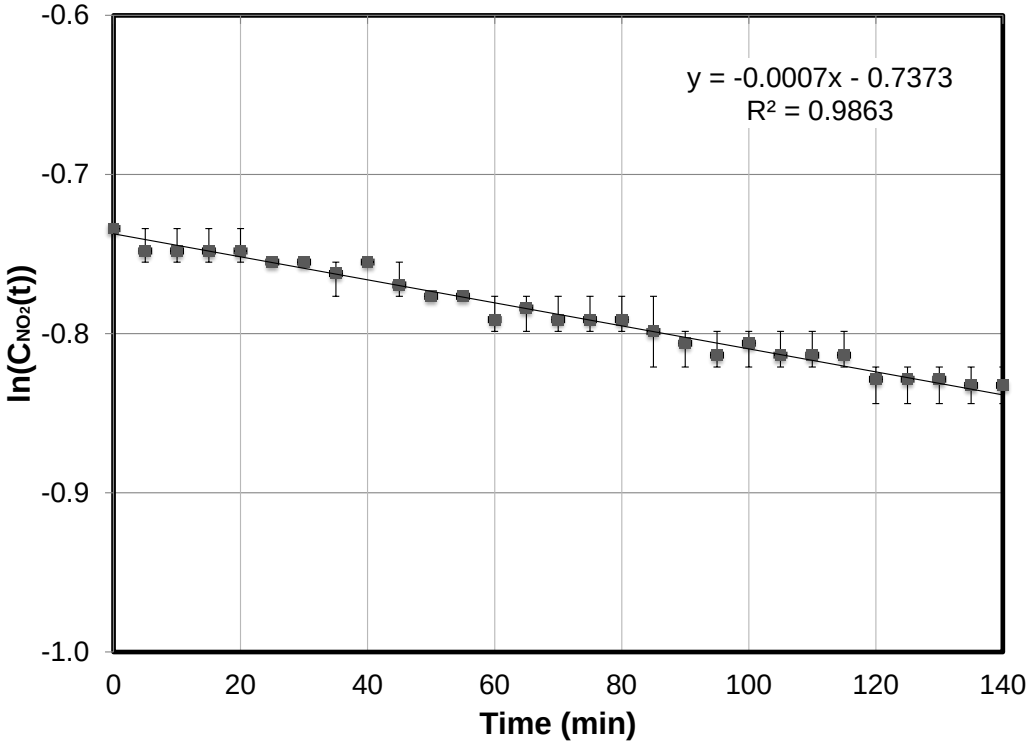

Figure 16 – NO_2 Removal Rate Control Test (No Localized Active Flow)

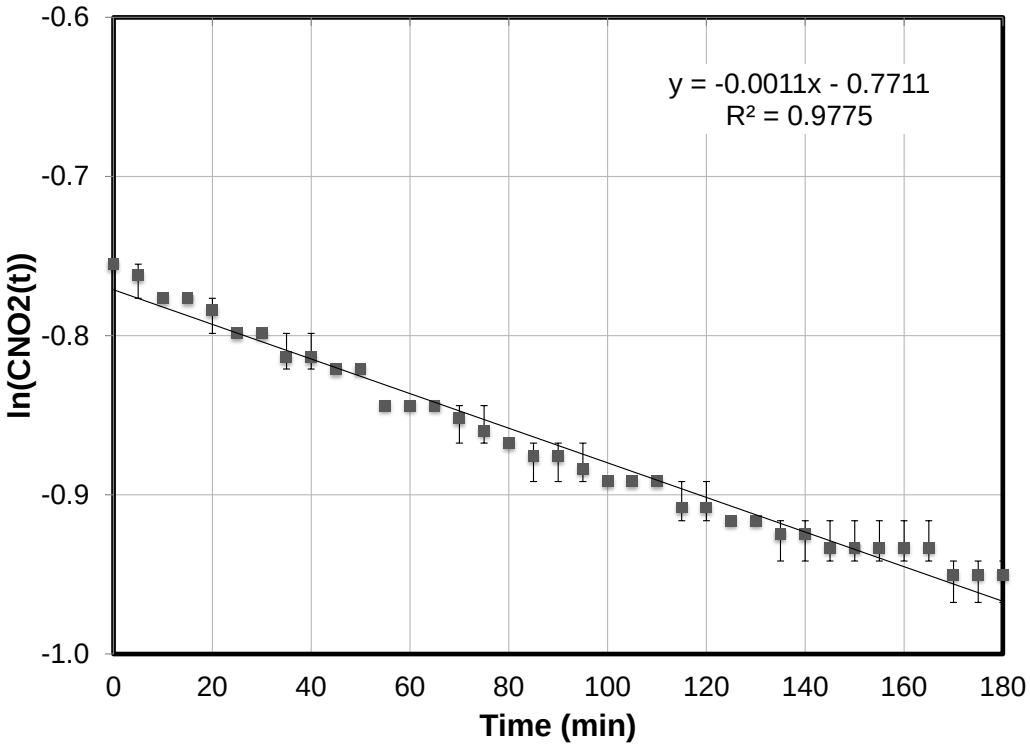

Figure 17 – NO_2 Removal Rate With Localized Active Flow (SJA) at L=115 mm

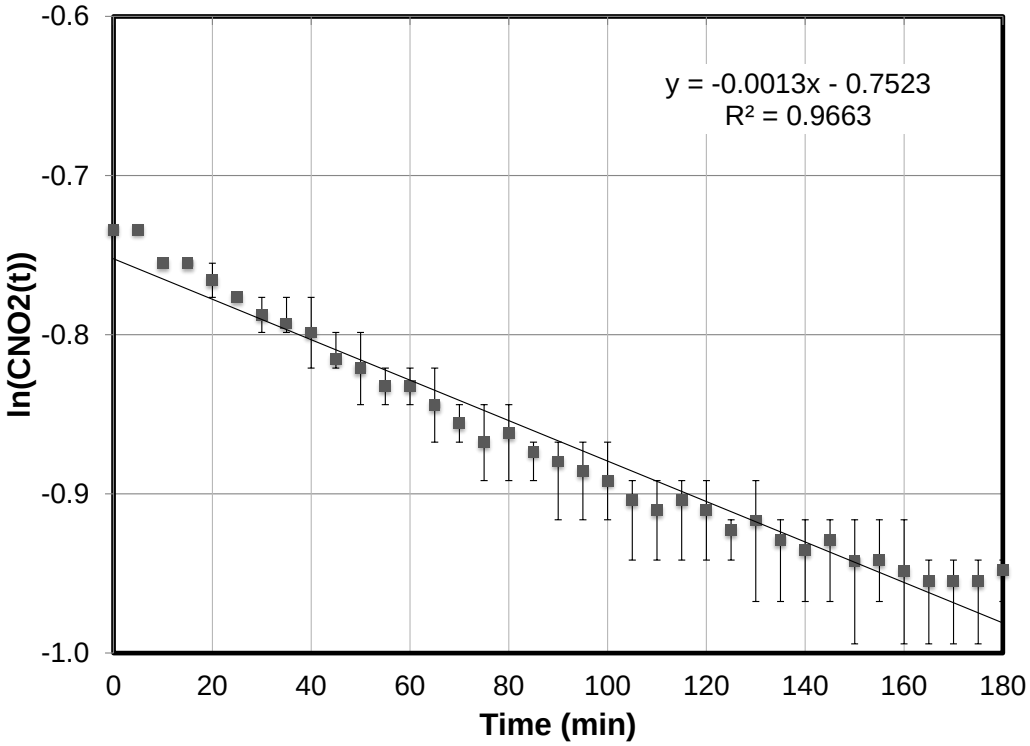

Figure 18 – NO_2 Removal Rate With Localized Active Flow (SJA) at L=315 mm

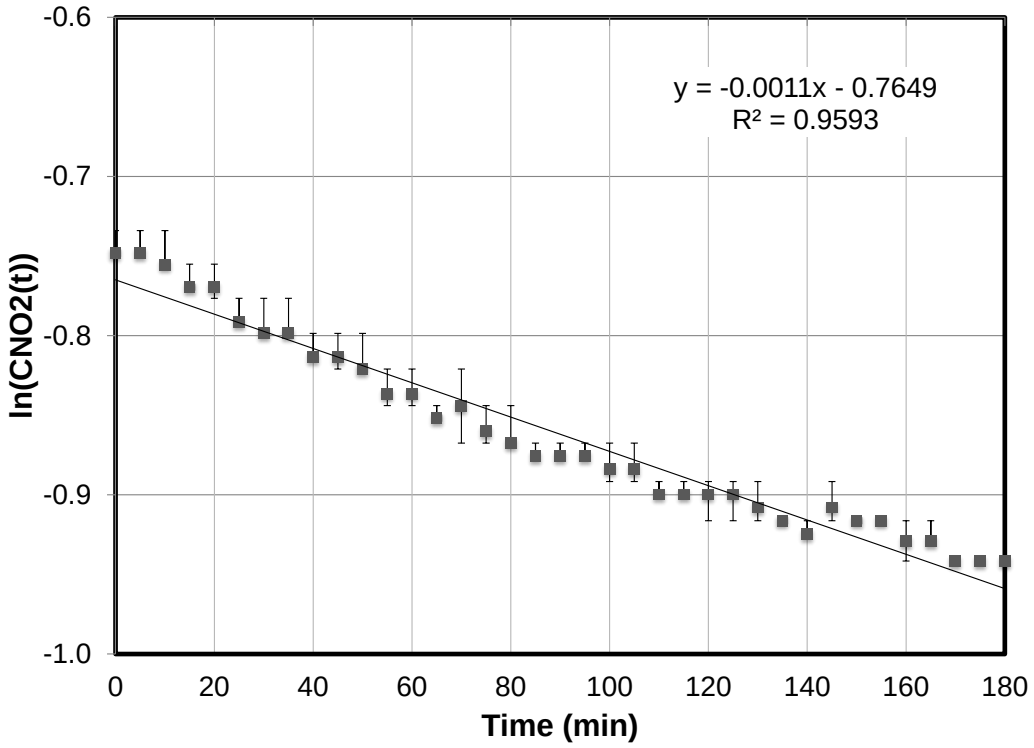

Figure 19 – NO_2 Removal Rate With Localized Active Flow (SJA) at L=510 mm

3.3.4 Comparison of devices with differing flow fields on pollutant removal

The experiment was repeated with the ACF at a distance of L=315 mm and the results are shown in Figure 20. The ACF generated a removal rate *k* of 0.0011 min^{-1}, which was equivalent to the removal rate of the SJA at L=115 mm (Figure 17) and L=510 mm (Figure 19). In Chapter 2, it was shown that both the SJA at L=510 mm and the ACF at L=315 mm generated a surface velocity of 0.1 m/s with a uniform distribution of velocities across the surface. However, it is interesting that the removal rate produced by these two similar conditions is equal to that of the SJA at L=115 mm, where the magnitude of the surface velocity was 0.4 m/s, with a steep decrease in velocity moving in the y and z directions across the surface. Since these three different conditions generated an equivalent removal, it appears that this process depends on other factors in addition to surface velocity magnitude and uniformity across the reactor.

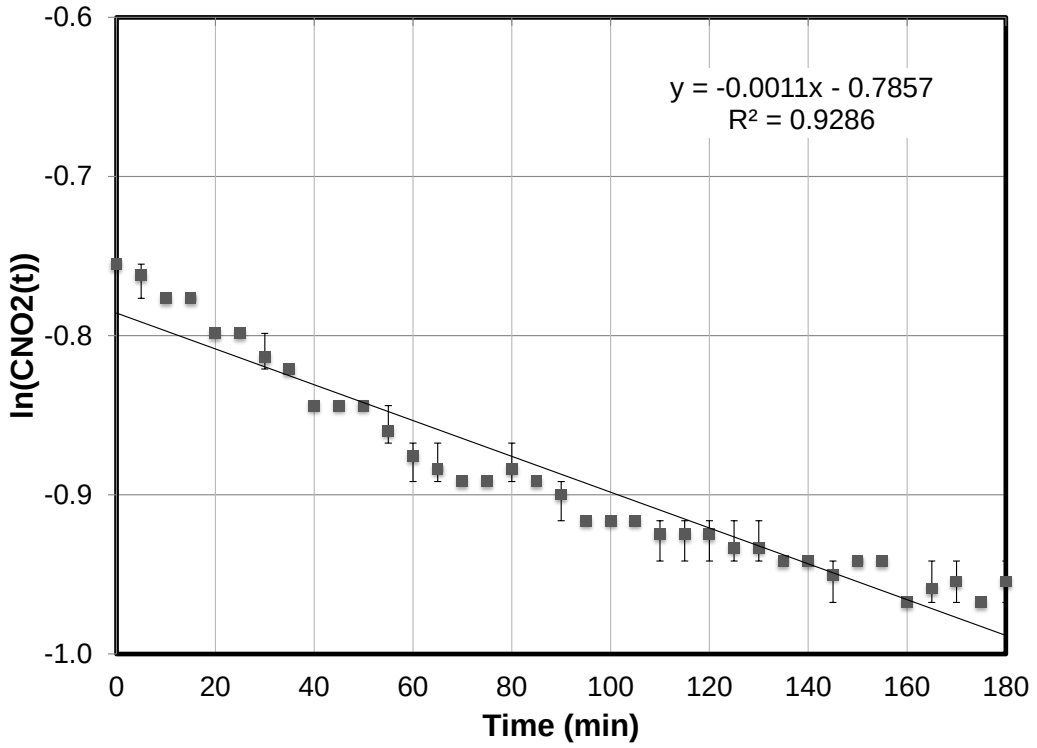

Figure 20 – NO_2 Removal Rate With Localized Active Flow (ACF) at L=315 mm

The ACF had a uniform flow field similar to the SJA at L=315mm. Additionally, the surface velocities of the ACF and SJA at 315mm were similar (0.1 m/s). Since the removal rate of the SJA (*k* of 0.0013 min^{-1}) was greater than that of the ACF (*k* of 0.0011 min^{-1}), it was determined that the flow regime of the ACF led to a lower removal rate. Table 3 summarizes the removal rate *k* values for all SJA L-distances as well as the ACF at 315 mm. These results show an 85.7% increase in the rate of removal of NO_2 using localized ventilation with the SJA at L=315, compared to the control case (no ventilation).

Table 3 – Summary of Removal Rates Determined for Photocatalytic Experiments

Active Flow Device	L-Distance (mm)	Removal rate *k* (min^{-1})	Removal rate *k* (hr^{-1})	Removal rate ($\mu gm^{-2}s^{-1}$)	Surface Velocity (ms^{-1})	Visual Velocity Distribution
none	-	0.0007	2.52	0.022	-	-
SJA	115	0.0011	3.96	0.031	0.40	Steep decline from surface center
SJA	315	0.0013	4.68	0.034	0.10	uniformly distributed
SJA	510	0.0011	3.96	0.031	<0.10	uniformly distributed
ACF	315	0.0011	3.96	0.031	0.10	uniformly distributed

Table 4 summarizes the percent of total NO_2 reduction over time. Percent reduction refers to the percent reduction in concentration from the initial concentration at time zero to the concentration at the stated time (10, 30, 60, 90, 120, 150, 180 min). The SJA at 115 mm and 510 mm resulted in similar reduction percentages over each time interval. This was an interesting result because, as discussed previously, the surface velocities at L=115 mm and L=510 mm were 0.4 m/s and <0.1 m/s respectively. Additionally, the higher airflow velocities at L=115 mm were concentrated near the centerline axis of the surface whereas at L=510 mm, the airflow velocities were uniformly distributed across the surface. This indicated that both velocity magnitude and distribution across the surface impact NO_2 removal rate. Moreover, the specific combination of the surface velocity at L=315 mm (0.1 m/s) and the uniformly distributed airflow across the surface of the reactor lead to the greatest removal rate.

The ACF had the highest percent reduction in the first hour of the experiment, but was surpassed by the SJA at L=315 mm in the remaining two hours. This result suggested that the reaction at the activated sites on the TiO_2-doped reactor surface was not enhanced by the greater turbulence level created by the ACF over prolonged periods of time; however, the initial chemical reactions may have been enhanced by the greater turbulence.

Table 4 - Percent of Total NO_2 Reduction

Time (min)	% Total NO_2 Reduction				
	No Active Flow Device (%)	**SJA at L=115 mm (%)**	**SJA at L=315 mm (%)**	**SJA at L=510 mm (%)**	**ACF at L=315 mm (%)**
10	1.39	2.13	2.08	0.70	2.13
30	2.08	4.26	5.21	4.93	5.67
60	5.56	8.51	9.38	8.45	11.35
90	6.94	11.35	13.54	11.97	13.48
120	9.03	14.18	16.15	14.08	15.60
150	10.42	16.31	18.75	15.49	17.02
180	12.50	17.73	19.27	17.61	18.09

3.3.4 Conclusions

As shown by the SJA at 115 mm, a higher velocity (0.4 m/s) at the center of the reactor surface resulted in a higher removal rate than the control, but lower removal rate than the optimized distance of the SJA at L=315 mm. The improvement over the control case may be attributed to enhanced air mixing near the reactor surface provided by the active flow device. Since the removal rates of the ACF at L=315 mm, SJA at 115mm, and SJA at 510 mm were equal, and, given their difference in surface velocity (0.4 m/s, 0.1 m/s, and 0.1 m/s respectively), it was determined that removal rate of NO_2 by TiO_2 does not increase with increasing surface velocity. Given the results of the removal rates found in Chapter 3, where the optimized location for removal of NO_2 via the TiO_2 reactor was the SJA at 315 mm, it can be concluded that the use of the active flow devices did enhance the removal rate of NO_2 over the control. The SJA at 315 mm resulted in the highest removal rate, where the velocity was near 0.1 m/s and nearly uniform across the surface. The same flow qualities, when produced by the ACF, resulted in a lower removal rate. Therefore it was concluded that the characteristics of the SJA vortices at the impingement surface contribute to the enhanced removal rate of NO_2 by TiO_2. These results contribute to the general understanding of photocatalytic removal of NO_2 by TiO_2 for low intensity illumination (interior) spaces. Since it is a low-power device with greater dynamic pressure than the ACF per unit input power (Abarr et al. 2016), the SJA therefore shows potential to be used in conjunction with air cleaning devices by enhancing air cleaning rates over ambient air while decreasing demand on energy intensive central HVAC systems.

CHAPTER 4:
FUTURE WORK

The results presented in this thesis are limited in nature but served as a proof of concept, particularly regarding the use of localized ventilation to enhance the photocatalytic removal of NO_2. Other parameters could be studied in order to optimize this approach to air quality control. For example, the angle of air impingement onto the reactor surface can be varied to determine whether there is additional enhancement at low angles, which can potentially extend the contact time between NO_2 and the photocatalytic surface. Varying the angle of air impingement will also add flexibility to location of implementation in buildings. Additionally, variation in mass of the photocatalyst and intensity of radiation on the surface has been proven to impact removal rates (Toma et al., 2004; Fujishima et al., 2000). If conducted in conjunction with varying the angle of airflow, characterization of surface velocity enhancement on pollutant removal may be better sensitized to these influential factors.

Altering the composition of the reactor base substance to be more or less permeable will also significantly impact surface velocities and therefore the overall findings. A more permeable surface will increase the number of available sites for catalysis. Furthermore, a continuation of the experimental analysis of surface roughness found in Chapter 2 might include characterization of the effect of surface roughness on photocatalytic removal rate.

Until recently, it was believed that UVA radiation was a necessity for TiO_2 photocatalytic activation. However, current research is moving towards the use of visible light (Fujishima and Zhang, 2006). In an ideal case, TiO_2 would be sensitive to visible light, which composes the largest portion of solar radiation. Fluorescent lamps mainly emit visible light, so the applications could extend well to electrically lit spaces. This potential transition to the use of visible light is critical to the implementation of TiO_2 in tunnels and building interiors. The addition of transition metal ions to TiO_2 (Cr_3+, Fe_3+) creates local energy levels within the band gap of the photocatalyst; therefore the ability of the material to absorb light, and by extension the photocatalytic reaction, is enhanced. Future work is needed to fully understand this

process, as some tests under these doping conditions showed no activity under visible light (Fujishima and Zhang, 2006). Anion doping is another method of shifting absorption range of TiO_2 to the visible spectrum. Results indicate that, although the shift can be done, the reaction rate is much lower than that of the same material under UV light. Future research is needed in this area to maximize the potential of the TiO_2 reactor within the preexisting conditions of building interiors.

Due to the existence of unwanted byproducts generated by the photocatalytic reaction of TiO_2 and NO_2, it is recommended for future experiments to use a combination of air cleaning materials so that all contaminants are addressed using a single reactor. Resolution in this area is especially critical given its potential as a localized air cleaner in building interiors.

CHAPTER 5
REFERENCES

Abarr, M., Mauney, D., Hertzberg, J.R., Montoya, L.D., 2016, “Characterization of a commercial synthetic jet actuator for air quality applications,” under review, Journal of Engineering Fluids.

Aghighi, A., Haghighat, F., 2015, “Evaluation of nano-titanium dioxide (TiO_2) catalysts for ultraviolet photocatalytic oxidation air cleaning devices,” Journal of Environmental Chemical Engineering, 3(3), pp. 1622-1629.

Allard, M.P., 2011. “Use of Synthetic Jets to Control Aerosol Dispersion in a Room,” Master’s Thesis, Rensselaer Polytechnic Institute, Troy, New York.

Arik, M., Setlur, A., 2009, "Environmental and economical impact of LED lighting systems and effect of thermal management," International Journal of Energy Research, 34, pp. 1195-1204.

ASTM D5116-10, Standard Guide for Small-Scale Environmental Chamber Determinations of Organic Emissions From Indoor Materials/Products, ASTM International, West Conshohocken, PA, 2010, www.astm.org

Ballari, M.M., Hunger, M., Husken, G., Brouwers, H.J.H., 2010, "NOx photocatalytic degradation employing concrete pavement containing titanium dioxide," Applied Catalysis B: Environmental, 95, pp. 245-254.

Barck, C., Lundahl, J., Hallden, G., Bylin, G., 2005, “Brief exposures to NO_2 augment the allergic inflammation in asthmatics,” Environ Res., 97, pp.58-66.

Bedjanian, Y., El Zein, A., 2012, "Interaction of NO_2 with TiO_2 Surface Under UV Irradiation: Products Study," The Journal of Physical Chemistry A, 116.7, pp. 1758-764.

Beeldens, A., Cassar, L., Murata, Y., 2011, "Applications of TiO_2 Photocatalysis for Air Purification," Rilem State of the Art Reports, 5, pp. 23-35.

Belanger, K., Holford, T.R., Gent, J.F., Hill, M.E., Kezik, J.M., Leaderer, B.P., 2013, “Household levels of nitrogen dioxide and pediatric asthma severity,” Epidemiology, 24, pp. 320-330.

Boonen, E., Beeldens, A., 2014, “Recent Photocatalytic Applications for Air Purification in Belgium,” Coatings, 4, pp. 553-573.

Burge, P.S., 2004, “Sick Building Syndrome,” Occup. Environ. Med., 61, pp. 185-190.

Carugno, M., Consonni, D., Randi, G., Catelan, D., Grisotto, L., Bertazzi, P.A., Biggeri, A., Baccini, M., 2016, “Air pollution exposure, cause-specific deaths and hospitalizations in a highly polluted Italian region,” Environmental Research, 147, pp. 415-424.

Chaudhari, M., Puranik, B., Argawal, A., 2011, "Multiple orifice synthetic jet for improvement in impingement heat transfer," International Journal of Heat and Mass Transfer, 54(9,10), pp. 2056-2065.

Chenari, B., Dias Carrilho, J., Gameiro da Silva, M., 2016, “Toward sustainable, energy-efficient and healthy ventilation strategies in buildings: A review,” Renewable and Sustainable Energy Reviews, 59, pp.1426-1447.

Cibella, F., Cuttitta, G., Della Maggiore, R., Ruggieri, S., Panunzi, S., De Gaetano, A., Bucchieri, S., Drago, G., Melis, M.R., La Grutta, S., Viegi, G., 2015, “Effect of indoor nitrogen dioxide on lung function in urban environment,” Environ Res., 138, pp. 8-16.

Daly, A. P. E., 2002, “Underfloor air distribution: lessons learned,” ASHRAE J., pp. 21.

Delfino, R.J., Staimer, N., Gillen, D., Tjoa, T., Sioutas, C., Fung, K., George, S.C., Kleinman, M.T., 2006, “Personal and ambient air pollution is associated with increased exhaled nitric oxide in children with asthma,” Environ Health Perspect., 114, pp. 1736-1743.

Emmerich, S.J., Persily, A.K., 1998, “Energy Impacts of Infiltration and Ventilation in U.S. Office Buildings Using Multizone Airflow Simulation,” IAQ and Energy, pp. 191-203.

Fisk, W. J., 2002, “How IEQ affects health, productivity,” ASHRAE J, 44(5), pp. 56–56.

Franklin, P., Runnion, T., Farrar, D., Dingle, P., 2006, “Comparison of peak and average nitrogen dioxide concentrations inside homes,” Atmospheric Environment, 40, pp. 7449-7454.

Fujishima, A. Rao, T.N., Tyrk, D.A., 2000, "Titanium dioxide photocatalysis," Journal of Photochemistry and Photobiology C: Photochemistry Reviews, 1, pp. 1-31.

Fujishima, A., Zhang, X., 2006, "Titanium dioxide photocatalysis: Present situation and future approaches," Comptes Rendus Chim., 9, pp. 750–760.

Glezer, A., Allen, M.G., Coe, D.J., Smith, B.L., Trautman, M.A., Wiltse, J.W., 1998, U.S. Patent No. 5758823. Atlanta, GA: U.S. Patent and Trademark Office.

Goswami, D.Y., Trivedi, D.M., Block, S.S, 1997, "Photocatalytic Disinfection of Indoor Air," Journal of Solar Energy Engineering, 119, pp. 92-96.

Hashimoto, K., Irie, H., Fujishima, A., 2005, “TiO_2 Photocatalysis: A Historical Overview and Future Prospects,” Japanese Journal of Applied Physics, 44(12), pp. 8269-8285.

Hodgson, A.T., Destaillats, H., Sullivan, D.P., Fisk, W.J., 2007, "Performance of ultraviolet photocatalytic oxidation for indoor air cleaning applications," Indoor Air, 17, pp. 305–316.

Hu, S., Shiue, A., Chang, S., Chang, Y., Tseng, C., Mao, C., Hsieh, A., Chan, A., 2016, “Removal of carbon dioxide in the indoor environment with sorption-type air filters,” International Journal of Low-Carbon Technologies, pp. 1-5.

Jokisalo, J., Kumitski J., Korpi, M., Kalamees, T. Viha J., 2009, “Building leakage, infiltration, and energy performance analyses for Finnish detached houses,” Building and Environment, 44(2), pp. 377-387.

Jorgensen, R.B., Bjorseth, O., Malvik, B., 1999, "Chamber Testing of Adsorption of Volatile Organic Compounds (VOCs) on Material Surfaces," Indoor Air, 9, pp. 2-9.

Kampa, M., Castanas, E., 2008, “Human health effects of air pollution,” Environmental Pollution, 151, pp. 362-367.

Katsanaki, A.V., Kontosa, A.G., Maggosb, T., Pelaezd, V.L., Pavlatouc, E.A., Dionysioud, D.D., Falarasa, P., 2013, “Photocatalytic oxidation of nitrogen oxides on N-F-doped titania thin films,” Applied Catalysis B: Environmental, 140-141, pp. 619-625.

Kjær, U. D., Tirkkonen, T., 1996, Summary of Adsorption/Desorption Experiments for the European Database on Indoor Air Pollution Sources in Buildings.

Knudsen, H.N., Kjaer, U.D., Nielsen, P.A., Wolkoff, P., 1999, "Sensory and chemical characterization of VOC emissions from building products: impact of concentration and air velocity," Atmospheric Environment, 33, pp. 1217-1230.

Lai, H.K., Bayer-Oglesby, L., Colvile, R., Gotschi, T., Jantunen, M.J., Kunzli, N., Kulinskaya, E., Schweizer, C., Nieuwenhuijsen, M.J., 2006, Determinants of indoor air concentrations of $PM_{2.5}$, black smoke and NO_2 in six European cities (EXPOLIS study)," Atmospheric Environment, 40, pp. 1299-1313.

Langridge, J.M., Gustafsson, R.J., Griffiths, P.T., Cox, R.A., Lambert, R.M., Jones, R.L., 2009, "Solar Driven Nitrous Acid Formation on Building Material Surfaces Containing Titanium Dioxide: A Concern for Air Quality in Urban Areas," Atmospheric Environment, 43(32), pp. 5128-5131.

Lasance, C.J.M., Aarts, R.M., 2008, "Synthetic Jet Cooling Part I: Overview of Heat Transfer and Acoustics," 24th IEEE SEMI-THERM Symposium.

Latza, U., Gerdes, S., Baur, X., 2009, "Effects of nitrogen dioxide on human health: Systematic review of experimental and epidemiological studies conducted between 2002 and 2006," Int. J. Hyg. Environ. Health, 212, pp. 271-287.

Li M., Shi J., Guo J., Cao J., Niu J., Xiong M., 2015, "Climate Impacts on Extreme Energy. Consumption of Different Types of Buildings," PLoS ONE., 10(4), e0124413. doi:10.1371/journal.pone.0124413.

Lu, C., Deng, Q., Li, Yuguo, Sundell, J., Norback, D., 2016, "Outdoor air pollution, meteorological conditions and indoor factors in dwellings in relation to sick building syndrome (SBS) among adults in China," Science of the Total Environment, 560-561, pp. 186-196.

Maddalena, R., Mendell, M. J., Eliseeva, K., Chan, W. R., Sullivan, D. P., Russell, M., Satish, U., Fisk, W. J. 2015, "Effects of ventilation rate per person and per floor area on perceived air quality, sick building syndrome symptoms, and decision-making," Indoor Air, 25, pp. 362–370.

Maggos, T., Bartzis, J.G., Leva, P., Kotzias, D., 2007, "Application of photocatalytic technology for NOx removal," Applied Physics A, 89, pp. 81-84.

Mao, N., Pan, D.M., Deng, S.M., Chan, M.Y., 2013, "Thermal, ventilation and energy saving performance evaluations of a ductless bed-based task/ambient air conditioning (TAC) system," Energy Build, 66, pp. 297–305.

Maury, A., De Belie, N., Demeestere, K., Mantyla, T., 2007, "Titanium dioxide containing cementitious materials: characterization and air cleaning potential," Proceedings of International RILEM Symposium on Photocatalysis, Environment and Construction Materials, pp. 227-234.

McQuillan, B.W., 2013. Synthetic Jet Flow Control in the Indoor Environment. Master's Thesis, University of Colorado, Boulder.

McQuillan, B., Hertzberg J. and Montoya L.D., 2014, "Flow Visualization Study of Synthetic Flow Control in the Indoor Environment", Building and Environment, 73, pp. 239-248.

Montoya L.D., Jackson J.L., Amitay M., 2010, "Control of Aerosol Dispersion and Removal in a Room Using Synthetic Jet Actuators," Building and Environment, 45, pp. 165–175.

Ng L., Persily A.K., Emmerick S.J., 2015, “IAQ and energy impacts of ventilation strategies and building envelope airtightness in a big box retail building,” Building and Environment, 92, pp. 627-634.

Ning, M., Dongmei, P., Shiming, D., Mingyin, C., 2013, “Thermal, ventilation and energy saving performance evaluations of a ductless bed-based task/ambient air conditioning (TAC) system,” Energy and Buildings, 66, pp. 297-305.

Park, S., Seo, J., Kim, J.T., 2015, “A study on the application of sorptive building materials to reduce the concentration and volume of contaminants inhaled by occupants in office areas,” Energy and Buildings, 98, pp. 10-18.

Pavlova, A., Amitay, M., 2006, "Electronic Cooling Using Synthetic Jet Impingement," Journal of Heat Transfer, 128, pp. 897-907.

Pavlova, A.A., Otani, K., Amitay, M., 2008, “Active control of sprays using a single synthetic jet actuator,” International Journal of Heat and Fluid Flow, 29, pp. 131-148.

Shaikh, K.A., Kale, S.S., Kashid, A.S., 2016, “Performance Evaluation of Synthetic Jet Cooling for CPU,” International Research Journal of Engineering and Technology, 3(1), pp. 728-731.

Smith, B.L., Swift, G.W., 2003, “A comparison between synthetic jets and continuous jets,” Experiments in Fluids, 34(4), pp. 467-472.

Spengler, J.D., Duffy, C.P., Letz, R., Tibbitts, T.W., Ferris, B.G.Jr., 1983, "Nitrogen Dioxide Inside and Outside 137 Homes and Implications for Ambient Air Quality Standards and Health Effects Research," Environmental Science and Technology, 17(3), pp. 164-168.

Spengler, J. D., McCarthy, J. F., and Samet, J. M., 2000, Indoor Air Quality Handbook, McGraw Hill Professional.

Tamburello, D.A., Amitay, M., 2008, “Active control of a free jet using a synthetic jet,” International Journal of Heat and Fluid Flow, 29, pp. 967-984.

Toma, F. L., Bertrand, G., Klein, D., Coddet, C., 2004, "Photocatalytic removal of nitrogen oxides via titanium dioxide," Environ Chem Lett., 2, pp. 117-121.

Travnicek, Z., Tesar, V., 2003, "Annular synthetic jet used for impinging flow mass-transfer," International Journal of Heat and Mass Transfer, 46, pp. 3291-3297.

Tunnicliffe, W.S., Burge, P.S., and Aryes, J.G., 1994, "Effect of domestic concentrations of nitrogen dioxide on airway responses to inhaled allergen in asthmatic patients," The Lancet, 344, pp. 1733-36.

Uhde, E., Salthammer, T., 2007, “Impact of reaction products from building materials and furnishings on indoor air quality—A review of recent advances in indoor chemistry,” Atmospheric Environment, 41, pp. 3111-3128.

USEPA Office of Air and Radiation, 2010, “Methane and Nitrous Oxide Emissions from Natural Sources.” Retrieved from http://nepis.epa.gov.

Webster, T., Bauman, F., and Reese, J., 2002, “Underfloor air distribution: thermal stratification,” Cent. Built Environ. [Online]. Available: http://escholarship.org/uc/item/9145t9gz.pdf.

Weschler, C.J., Little, J.C., 2007, “Chemical and physical factors that influence pollutant dynamics in indoor atmospheric environments,” Atmospheric Environment, 41, pp. 3109-3110.

Wilkins, K., Wolkoff, P., Knudsen, H.N., Clausen, P.A., 2007, "The impact of information on perceived air quality – 'organic' vs. 'synthetic' building materials," Indoor Air, 17, pp. 130-134.

Wolkoff, P., Clausen, P.A., Jensen, B., Nielsen, G.D., Wilkins, C.K., 1997, "Are we measuring the relevant indoor pollutants?," Indoor Air, 7, pp.92-106.

Zhang, J. S., Zhang, J. S., Chen, Q., 2002, "Modeling VOC sorption of building materials and its impact on indoor air quality," ASHRAE RP-1097 Phase I. American Society of Heating, Refrigerating, and Air Conditioning Engineers, Atlanta.

Ziegler J., 2007, Active Control of Air Quality Using Synthetic Jet Actuators. Master's Thesis, Rensselaer Polytechnic Institute, Troy, New York.